

Variations in Mineral Abundance within a Single Horizontal Well Path in the Woodford Shale,
Arkoma Basin, Oklahoma

by

Tyrel David Wehner

B.S., Wichita State University, 2015

A THESIS

submitted in partial fulfillment of the requirements for the degree

MASTER OF SCIENCE

Department of Geology
College of Arts and Sciences

KANSAS STATE UNIVERSITY
Manhattan, Kansas

2018

Approved by:

Major Professor
Matthew Totten

Copyright

© Tyrel Wehner 2018.

Abstract

The Woodford Shale (Oklahoma, U.S.A.) is a prolific unconventional hydrocarbon resource. The Woodford has been shown to be heterogeneous in many geochemical, mineralogical, and rock mechanic properties across the state of Oklahoma, which presents a challenge to successful exploitation of this resource (Caldwell, 2014; Turner et al., 2015; Wiley, 2015; Zhang et al., 2017). Most prior studies of the Woodford Shale report properties from a single sample collected from a vertical well, which reports these values as a single point source on a distribution map. Studies using outcrop localities report lateral variations in several rock properties of the Woodford, but are limited to the short distances an outcrop provides (Turner et al., 2015).

The main focus of this research is to determine whether rock properties important to the productivity of the Woodford Shale vary across a lateral well bore within the Woodford shale. Measurements of chemical and mineralogical compositions were performed on rock cutting samples from a single horizontal well path of the Carleigh 6H-32 across approximately one mile. The mineral makeup was determined by use of X-ray diffraction (XRD) and elemental concentrations were determined by hand-held X-ray fluorescence (HHXRF). What was found is that the Upper and Middle Woodford Shale are relatively homogeneous laterally. The lack of variation means that it's possible to determine from which subgroup samples may have been taken. The geochemical data were used to calculate a mineral-based brittleness index (Wang and Gale, 2009), which was compared to the measured frack gradient across perforations of the Carleigh 6H-32 well. In addition, the total organic matter content (TOC) was approximated in the same samples using loss on ignition (LOI) methods.

The calculated mineralogy within samples assigned to the Middle Woodford show some variability throughout the horizontal well, which leads to an associated variation in mineral brittleness index when using the Wang and Gale (2009) formula. The mineral based brittleness index correlates with observed fracture gradient during well completion. This suggests that the tendency to fracture is also variable along the well path, which should be considered during design of the well completion.

Table of Contents

List of Figures	vii
List of Tables	ix
Acknowledgements	x
Dedication	xi
Chapter 1 - INTRODUCTION	1
Chapter 2 - GEOLOGICAL SETTING	6
2.1 - THE WOODFORD SHALE	6
2.2 - WOODFORD SHALE MEMBERS	9
2.2.1 - Lower Woodford Shale Member	9
2.2.2 - Middle Woodford Shale Member	9
2.2.3 - Upper Woodford Shale Member	9
2.3 - THERMAL MATURITY OF THE WOODFORD SHALE	10
2.4 - TOTAL ORGANIC CONTENT OF WOODFORD SHALE	12
Chapter 3 - HYPOTHESIS	14
Chapter 4 - METHODOLOGY	15
4.1 - Handheld X-Ray Fluorescence	15
4.2 – Bulk Powder X-Ray Diffraction	16
4.3 - Loss on Ignition (as a proxy for TOC)	16
Chapter 5 - RESULTS	18
5.1 - HHXRF Results	18
5.2 – XRD Results	20
5.3 – Loss on Ignition Results	23
Chapter 6 - DISCUSSION	25
6.1 – Calculated Mineralogy	25
6.2 - Mineral Brittleness Index	29
6.3 - Frack Gradient and Mineral Brittleness Index	31
Chapter 7 - CONCLUSION	35
References	36
Appendix A - HHXRF Table Concentrations	42

Major HHXRF Elemental Concentrations.....	42
Minor HHXRF Elemental Concentrations	45
Appendix B - XRD Bulk Powder Data.....	47
Appendix C - Loss on Ignition Data Tables	58
Appendix D - Weight percent of calculated mineralogy	61

List of Figures

- Figure 1. The lower 48 state shale plays (EIA, 2014). 1
- Figure 2. Map of Oklahoma showing present day tectonic and depositional provinces and the Coalgate Township 32, NE along with pointing to the location in Coal County of Pablo Carleigh wells, shown by the star. The area of study is within the Arkoma Basin, which is bounded by the Cherokee Platform and Ozark Uplift to the north, the Arbuckle Uplift to the west, the Ouachita Uplift to the south and the Mississippi Embayment to the east (Modified from Northcutt and Campbell, 1995; Oklahoma Geological Society, 2004). 4
- Figure 3. Pablo Carleigh Area Map, from Pablo Energy. This is a standard map view as if viewed from an airplane. The Pablo Carleigh 6H-32 is circled for easy locating. Each square represents a section that is 640 acres and is one mile wide by one mile high (USGS, 2017). The blue lines represent wellpath that are not owned by Pablo Energy. The orange/red lines represent Pablo Energy owned wellpaths. The thick black lines represent faults and the knob on those lines represent fault direction and dip..... 5
- Figure 4. Stratigraphic column of Oklahoma, showing the Woodford Shale sitting on top of the Hunton Group unconformity, the red oval is to highlight the focus of the study (Portas, 2009). 7
- Figure 5. Late Devonian Map of the United States, lower 48 states (modified from Blakey, 2016). 8
- Figure 6. Isopach map showing thickness of the Woodford Shale in Oklahoma and Arkansas (Boyd, 2006). The black dotted line outlines the Coastal Plain. The red line with the triangles define the Ouachita Thrust (Northcutt and Campbell, 1995)..... 8
- Figure 7. Characteristics defining the Upper, Middle, Lower Woodford Shale described from modified Hester et al., 1990; Lambert, 1993; Comer, 2008; Turner et al., 2015b..... 10
- Figure 8. Isoreflectance vitrinite map of eastern Oklahoma indicating gradient change throughout the Arkoma Basin, overlain with the top 10 major operators 2004-2008; the blue star is the approximate location of the well (modified from Cardott, 2008). 11
- Figure 9. The wt% total organic carbon for Woodford Shale in Oklahoma and western Arkansas, the blue star is the approximate location of the well of this study (Comer, 2008). The black

dotted line outlines the Coastal Plain. The red line with the triangles are to define Ouachita Thrust (Northcutt and Campbell, 1995).....	12
Figure 10. A scatter diagram of percent ignition loss at 550° C and percent organic carbon (modified from Dean, 1974).	17
Figure 11. Major Elements	18
Figure 12. Trace Elements	19
Figure 13. Bulk XRD diffractogram, sample 6820 example	20
Figure 14. TOC across the wellpath, yellow is Hunton Limestone.	24
Figure 15. Wt% calculated mineralogy vs distance along the wellpath, with an interpretation based on the calculated mineralogy.	26
Figure 16. Wellpath of Pablo Carleigh 6H-32. The abbreviations are as follows: FSL, Feet South Line; FNL, Feet North Line, these are used mainly to ensure operators are not taking resources they did not lease or own beyond their line, WDFD A1, Upper Woodford Shale; WDFD A2, Middle Woodford Shale; Lwr. WDFD, Lower Woodford Shale; MD, Measured Distance. The red line at the bottom is the resistivity curve and the green line at the bottom is the gamma ray.	28
Figure 17. Mineral Brittleness Index formula used from (Wang and Gale, 2009).....	29
Figure 18. Mineral Brittleness Index as per Wang and Gale (2009) across the wellpath, excluding the Hunton Limestone	30
Figure 19. Quartz (wt%) vs MBI variation.....	30
Figure 20. MBI versus frack gradient. Upper Woodford Shale in red and Middle Woodford Shale in blue.....	33
Figure 21. Middle Woodford Shale samples MBI versus frack gradient can estimate	34

List of Tables

Table 1. Mineral XRD interpretation of abundance. The legend for the table: X – minerals are minimally present to present, XX – minerals are common, XXX – minerals are abundant. The Hunton Limestone is indicated with an asterisk next to the sample number, otherwise the rest of the samples are identified as Woodford Shale.	22
Table 2 - TOC information statistics.	23
Table 3. MBI Statistical Information of the Woodford Shale	31
Table 4. Stage and perforating information along with a list of samples used to generate MBI; modified from Pablo Carleigh (2014).....	32

Acknowledgements

I would like to thank Dr. Totten for his excellent guidance. I would like to thank my advisors for their support, Dr. Abdelmoneam Raef, Dr. Sambhudas Chaudhuri, and Dr. Pamela Kempton. I would like to thank Colleen Gura for assistance in the use of the XRD and HHXRF for this study. I would like to thank Dr. Brice Lacroix for use of his lab for LOI.

Dedication

I would like to dedicate this thesis to my family without their support I would have never been able to complete this.

Chapter 1 - INTRODUCTION

Shales comprise nearly two-thirds of the Earth’s sedimentary record and some can contain oil and gas (Potter et al., 1980). Recent engineering developments that have been able to establish artificial permeability in shales have significantly enhanced the economic potential of unconventional oil and gas reserves. Industrial activity in the continental United States reflects this trend of increased economic potential. For example, in 2014 natural dry gas production was 12.3 trillion cubic feet, whereas in 2016 natural dry gas production increased to 15.8 trillion cubic feet (EIA, 2014, 2017). As a result of these technological developments, production of tight natural gas is expected to become an increasingly higher percentage of dry gas production in the continental United States. The utilization of horizontal wells lies behind much of this increase in dry natural gas production, by increasing the accessibility of these shale resources (EIA, 2014). They also present a new opportunity for research in terms of characterizing the lateral variability and complexity of mudrocks in a way that was not previously possible (Totten, 2011). The distribution of current shale plays of the lower 48 United States is shown in Figure 1.

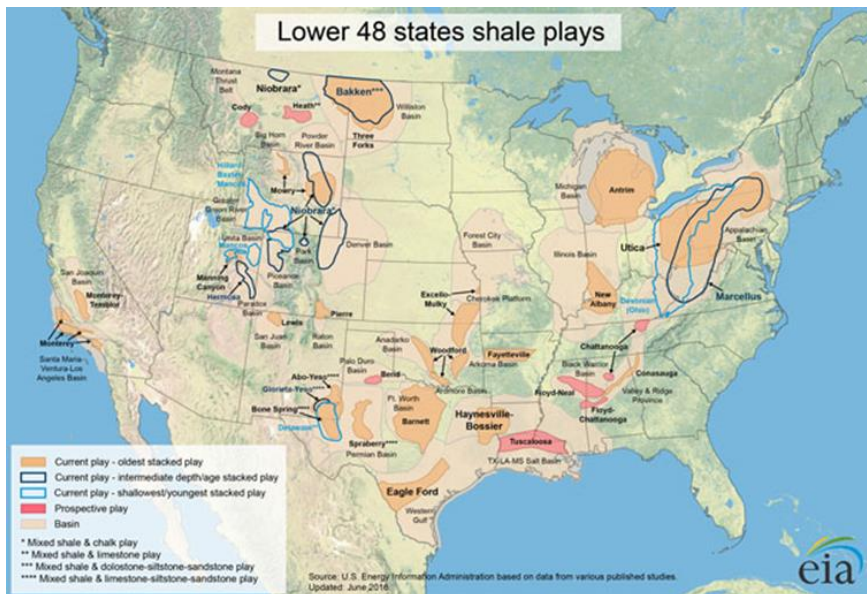


Figure 1. The lower 48 state shale plays (EIA, 2014).

In spite of the fact that mudrocks comprise over 60% of the sedimentary column, they are less understood than coarser grained siliciclastic sediments (Totten and Hanan, 1998). The petrology of mudrocks has historically focused on the clay-mineral fractions, while the non-clay fraction has received less attention. Two studies that have focused on the quartz and feldspar fractions in mudrocks include Kirkland et al. (1992) and Totten and Blatt (1993). The subgroup characteristics will be discussed in further detail within the geological section.

Whole-rock geochemical studies of mudrocks have tried to establish the relationship between trace element chemistry and provenance (Condie, 1991; Totten et al., 2000), but most of these studies did not consider organic-rich mudrocks. An exception is the recent study by Turner et al. (2015a,c), who examined the organic-rich Woodford Shale to gain an understanding of trends between elemental composition and total organic matter. They showed that organic-rich Woodford Shale has distinct trace element signatures, such as elevated molybdenum or vanadium contents, that correlate strongly with organic matter content (Turner et al. 2015c); these compositional variations are believed to have been influenced by basin water conditions (Tribovillard et al., 2015; Zhang et al., 2017). Therefore, Mo and V concentrations can be used in some cases for stratigraphic correlation (Tribovillard et al., 2006; Turner et al., 2015c).

One of the gaps in these previous studies is that they consider variations in shale composition across a regional area, but rarely incorporate sample variations within a smaller sample area. How do we know that there is not a significant difference in the samples across a large outcrop, or even from within the next ten feet of horizontal drilling? Are regional maps, constructed on the basis of vertical well data, truly representative of the variation in shale composition, or should we consider them as averages of a more diverse rock composition across a more limited area? Lateral variability is important for developing strategies for fracking, and

horizontal wells potentially can provide understanding of this lateral variation. However, variations in elemental compositions, total organic matter, and mineralogy within shales have not been reported in horizontal wells. Studies utilizing vertical wells have been conducted that use a single point (one sample per well) (Wall, 2015; Wiley, 2015). Vertical well cores have also been studied to generate standards for chemostratigraphy to generate a reference range for shales of the Barnett Basin (Rowe et al., 2010). The drawback of such studies is that they lack the potential of horizontal well counterparts to provide information about lateral heterogeneity. Values across the lateral penetration of a well could provide meaningful data by relating the elemental compositions, total organic matter, and mineralogy within an individual well, which could enable enhanced gas recovery within a single horizontal well (Turner et al. 2015a,b,c).

The research in this thesis addresses this question of lateral compositional variability in shales. Pablo Energy provided samples from the Pablo Carleigh 6H-32, a horizontal well that intersects the Upper and Middle Woodford Shale and remains continuously within these units for almost a mile. The Pablo Carleigh 6H-32 well is therefore ideal for this study, because it provides a unique opportunity to examine rock cuttings for lateral variations along reasonably consistent stratigraphic positions within the Woodford (Figure 2). A map of well paths in the area shows that the Pablo Carleigh crosses a fault and extends throughout the mile section (USGS, 2017) (Figure 3).

These data are compared to previous studies using samples collected from outcrops or multiple wells within a single area to examine whether a single point on a map is representative of a regional area, i.e. are there changes within a short distance of a mile at depth within a single well path? The outputs from this study should assist in maximizing the recoverable energy of the Woodford Shale in two ways: (1) through increased understanding of the lateral variation in

shale petrology in a localized area, and (2) by demonstrating the validity of new geochemical tools for pinpointing ideal locations within a horizontal well drilling range to perforate, i.e. areas that are richest in organic content and with the highest frackability.

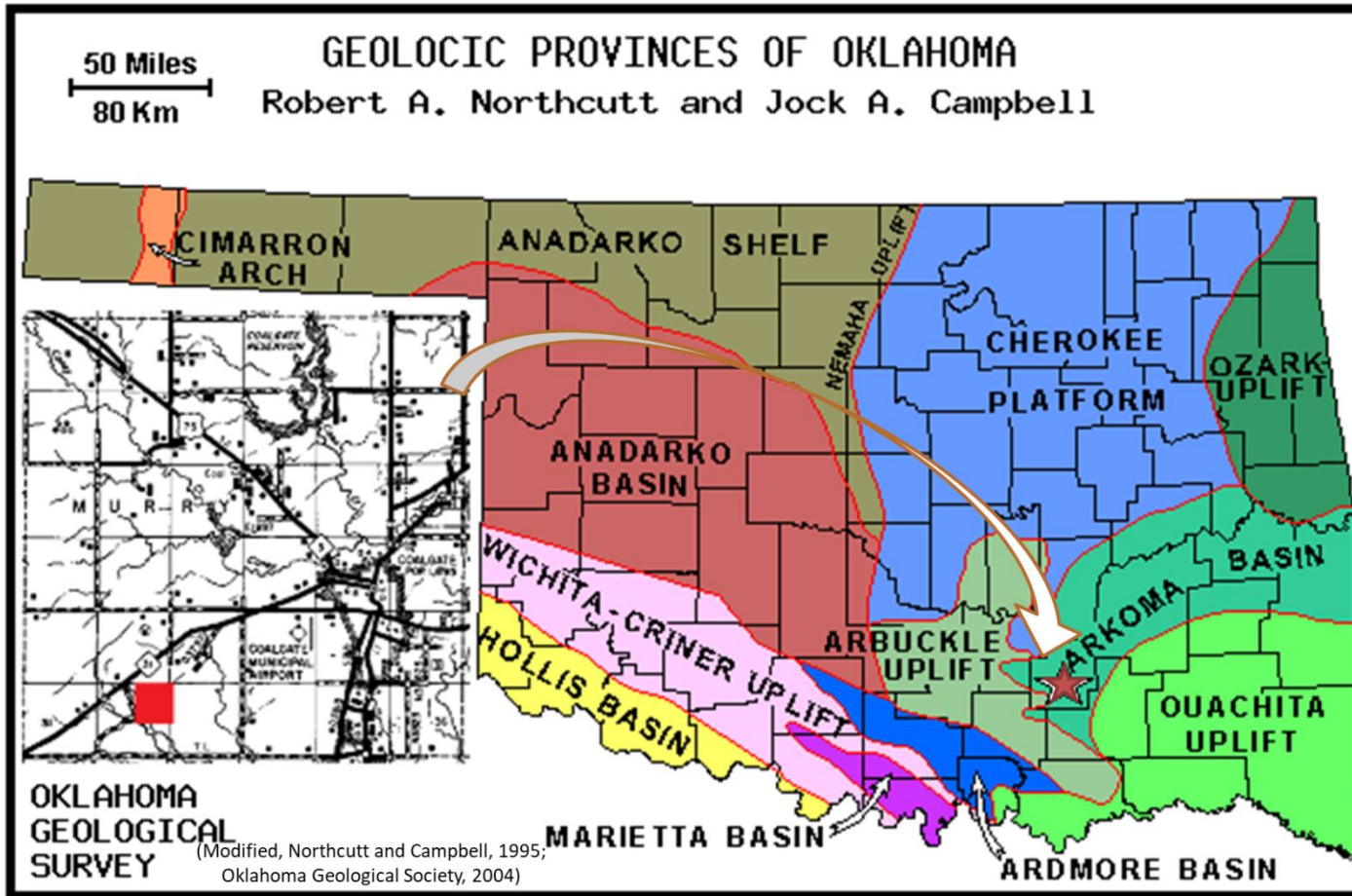


Figure 2. Map of Oklahoma showing present day tectonic and depositional provinces and the Coalgate Township 32, NE along with pointing to the location in Coal County of Pablo Carleigh wells, shown by the star. The area of study is within the Arkoma Basin, which is bounded by the Cherokee Platform and Ozark Uplift to the north, the Arbuckle Uplift to the west, the Ouachita Uplift to the south and the Mississippi Embayment to the east (Modified from Northcutt and Campbell, 1995; Oklahoma Geological Society, 2004).

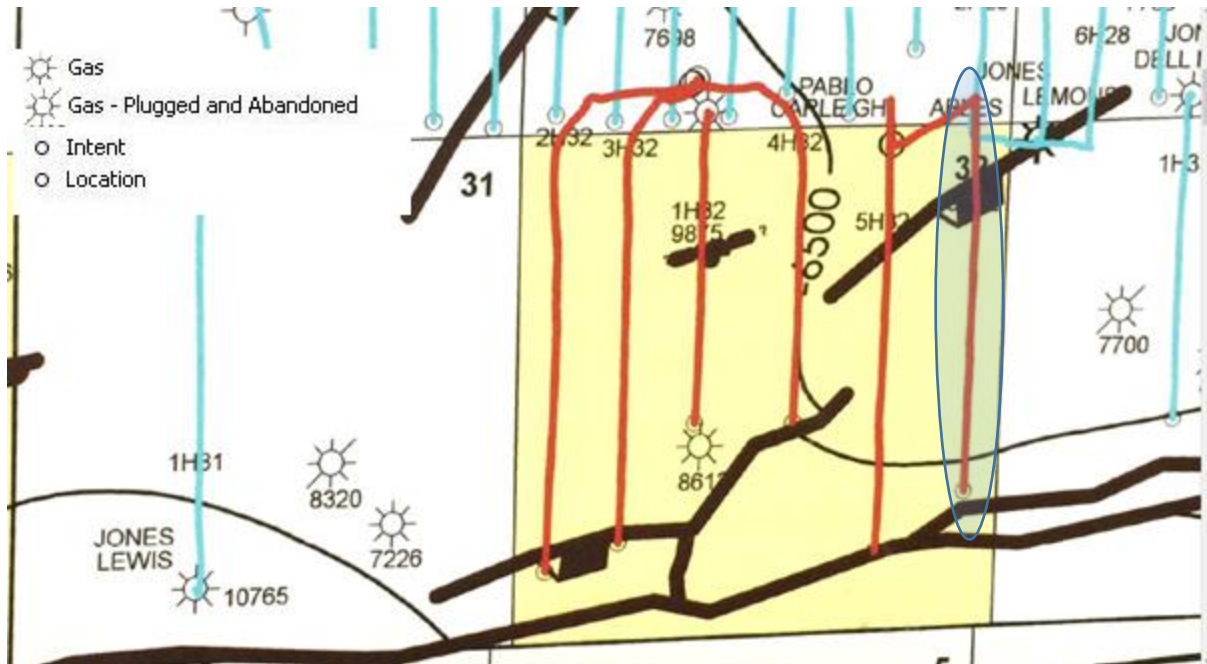


Figure 3. Pablo Carleigh Area Map, from Pablo Energy. This is a standard map view as if viewed from an airplane. The Pablo Carleigh 6H-32 is circled for easy locating. Each square represents a section that is 640 acres and is one mile wide by one mile high (USGS, 2017). The blue lines represent well path that are not owned by Pablo Energy. The orange/red lines represent Pablo Energy owned well paths. The thick black lines represent faults and the knob on those lines represent fault direction and dip.

Chapter 2 - GEOLOGICAL SETTING

The Arkoma Basin consists of Cambrian to Pennsylvanian age rocks that are rich in hydrocarbons. Tectonic features that define the Arkoma Basin are the Wichita Aulacogen and Ouachita Trough (U.S. Department of Energy, 1981; Denison et al., 1989; Walper, 1976).

The Wichita Aulacogen, previously known as the Southern Oklahoma geosyncline (Walper, 1976), is located in southern Oklahoma. It represents the failed rift arm of a triple junction that would become the Iapetus spreading center (Hanson et al., 2013). It developed on Precambrian granite basement during the Cambrian. The rift arms closed approximately 300 million years ago and formed part of the Ouachita orogenic belt (Denison et al., 1989; Hanson et al., 2013).

The Southern Oklahoma Aulacogen is an area that had significant uplift that created a graben, an area of crustal thinning (Ham et al, 1964; Walper, 1977; Brewer et al., 1983; Keller et al., 1983). Garner and Turcotte (1984) noted that the rate of subsidence slowed during the Middle Pennsylvanian Period and throughout the Permian Period. The Southern Oklahoma Aulacogen ceased forming in the Permian, as shown by Garner and Turcotte (1984). The importance of the Southern Oklahoma Aulacogen in relationship to the Arkoma Basin is that it created a deep basin where abundant deposition could occur.

2.1 - THE WOODFORD SHALE

The Woodford Shale, which is located throughout Oklahoma (Figure 4), is deep marine black shale that was deposited during the Late Devonian Period through the Early Mississippian Period (Figure 5) (Amsden, 1975; U.S. Department of Energy, 1981; Lambert, 1993). The Woodford Shale was deposited during the Kaskaskia I transgression (Lambert, 1993). The Kaskaskia I

transgression began during the Late Devonian and ceased during the Early Mississippian period (Monroe, 1997).

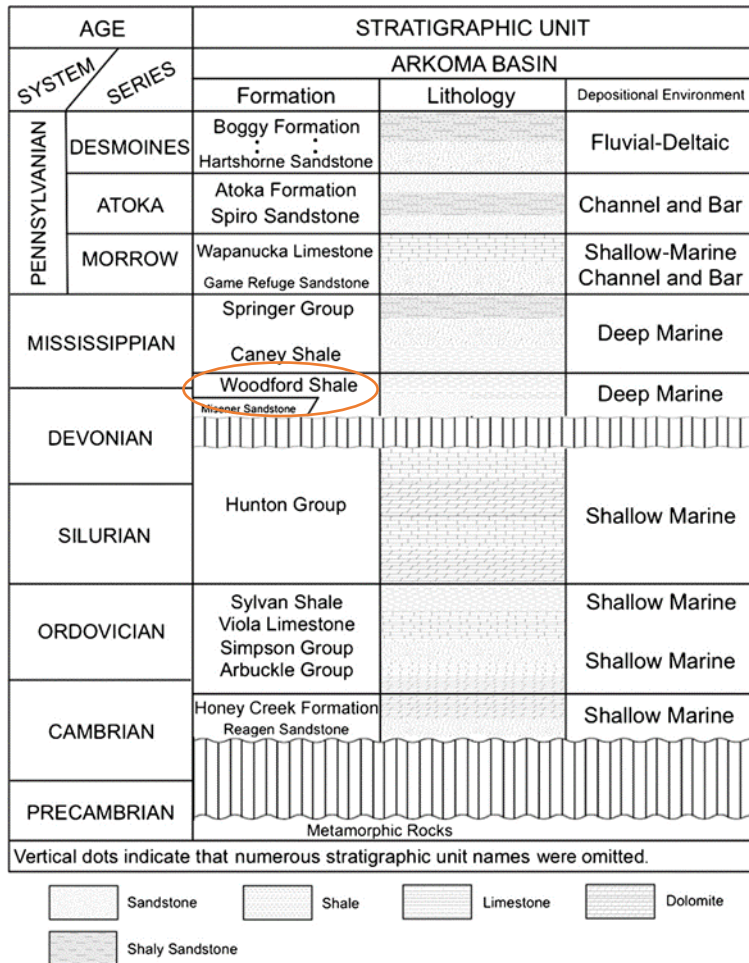


Figure 4. Stratigraphic column of Oklahoma, showing the Woodford Shale sitting on top of the Hunton Group unconformity, the red oval is to highlight the focus of the study (Portas, 2009).

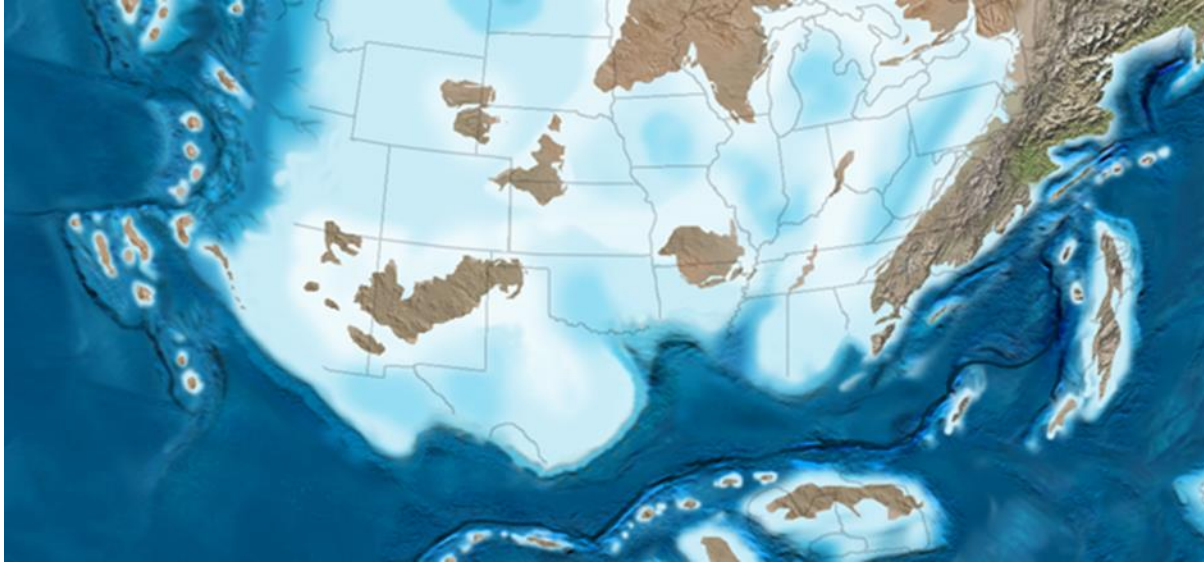


Figure 5. Late Devonian Map of the United States, lower 48 states (modified from Blakey, 2016).

The Woodford Shale reaches between 300 to 400 feet maximum thickness in southwestern Oklahoma (Figure 6), and thins to less than 50 feet towards the north (Boyd, 2006). It is subdivided into three members, lower, middle, and upper (Lambert, 1993.). These units are described below.

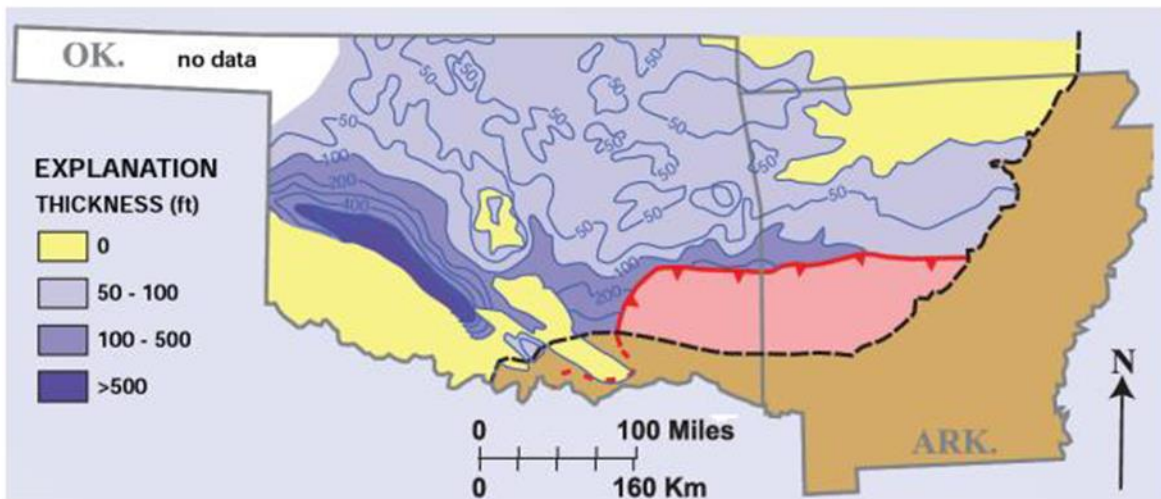


Figure 6. Isopach map showing thickness of the Woodford Shale in Oklahoma and Arkansas (Boyd, 2006). The black dotted line outlines the Coastal Plain. The red line with the triangles define the Ouachita Thrust (Northcutt and Campbell, 1995).

2.2 - WOODFORD SHALE MEMBERS

2.2.1 - Lower Woodford Shale Member

The Lower Woodford Shale is the least widespread of the Woodford Shale members, but is located sporadically throughout Oklahoma and South Central Kansas. The lower shale has a distinctive identifiable mineralogy; its composition includes quartz, silt (light), and abundant clay matrix, with glauconite silt (gray) being present (Figure 7). The greatest thickness is 150 feet found in southern Oklahoma (Lambert, 1993).

2.2.2 - Middle Woodford Shale Member

The Middle Woodford Shale has the greatest areal extent of the three shale members: it is found throughout Oklahoma as well as eastern Kansas. The middle member is also the thickest, with thicknesses up to 200 feet in the McPherson Valley of Central Kansas (Lambert, 1993; Lee, 1940; 1956). Most hydrocarbon production comes from the middle Woodford. Petrographic examination suggests that quartz silt is rare in samples from south-central Oklahoma (Lambert, 1993).

2.2.3 - Upper Woodford Shale Member

The Upper Woodford Shale is the second largest member in terms of area, more extensive than the lower member, but less extensive than the middle member. It is found throughout Oklahoma and central Kansas, extending up to 150 feet thick at its thickest part within the McPherson Valley area of central Kansas. The upper shale contains abundant silt-size dolomite (Lambert, 1993).

To summarize, the most abundant minerals in the Woodford Shale are quartz, which ranges from 29-87 %, and illite, which ranges from 8-35 %. Dolomite abundance ranges from

0-56 %. Other minerals of the Woodford Shale occur in abundances of 10 % or less, and include pyrite, kaolinite, and phosphate nodules. The Woodford Shale is described as being rich in biogenic quartz from radiolarians and sponge spicules (Kirkland et al., 1992).

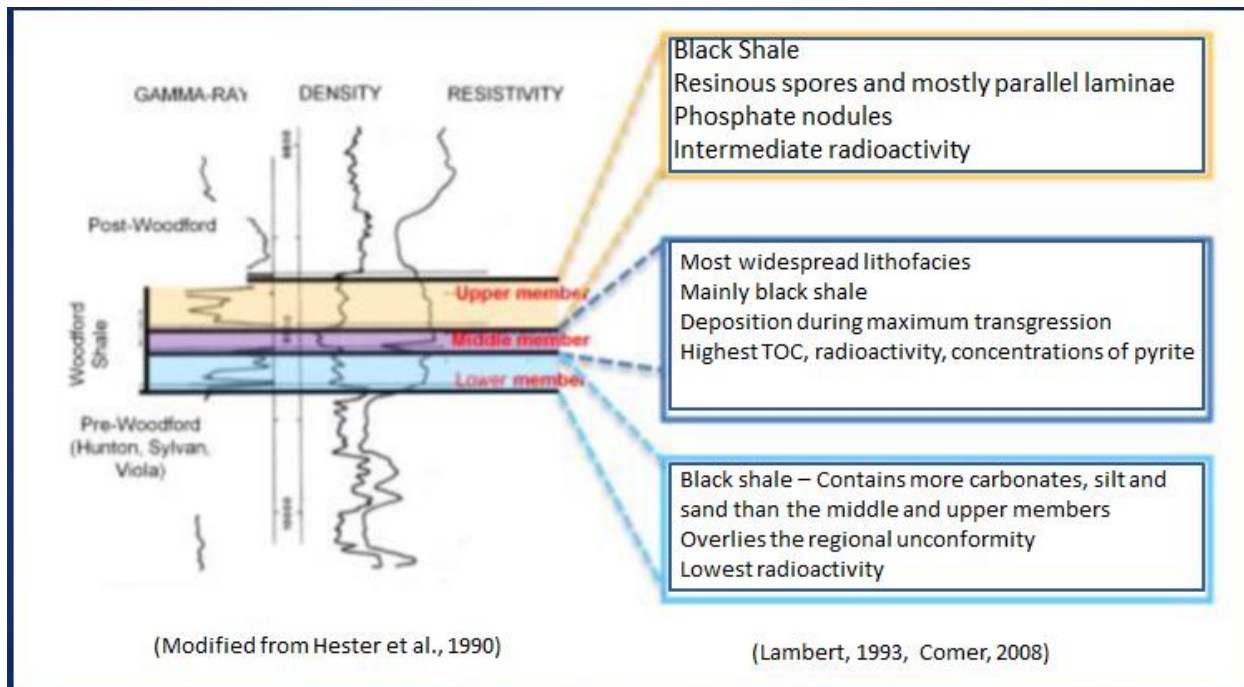


Figure 7. Characteristics defining the Upper, Middle, Lower Woodford Shale described from modified Hester et al., 1990; Lambert, 1993; Comer, 2008; Turner et al., 2015b.

2.3 - THERMAL MATURITY OF THE WOODFORD SHALE

Analysis of thermal maturity is used to infer whether organic shale is likely to produce oil and/or gas. One way to assess thermal maturity is by measuring the amount and reflectance of a vascular plant tissue called vitrinite. This is accomplished by measuring the reflectance as a percentage of the light that is reflected from the vitrinite found in organic-rich shales (Cardott and Lambert, 1985; Andrews, 2009; Cardott, 2012).

Thermal maturity of the Woodford Shale within the Arkoma Basin typically ranges from 1.0-3.0% vitrinite reflectance, R_v. Exploratory wells in the deepest part of the Arkoma Basin, still within the Woodford Shale, have R_v values of 3.0% and are known to contain saturated gas

(Houseknecht, 2014). The typical thermal maturity range of oil is 0.5 to 1.35% Rv; condensate is 0.85 to 2.0% Rv; dry gas is 1.0-3.0% Rv (Dow, 1977). Typically, thermal maturity in the Arkoma Basin is observed as a gradient and does not exhibit abrupt changes, as seen in Figure 8 (Cardott, 2008).

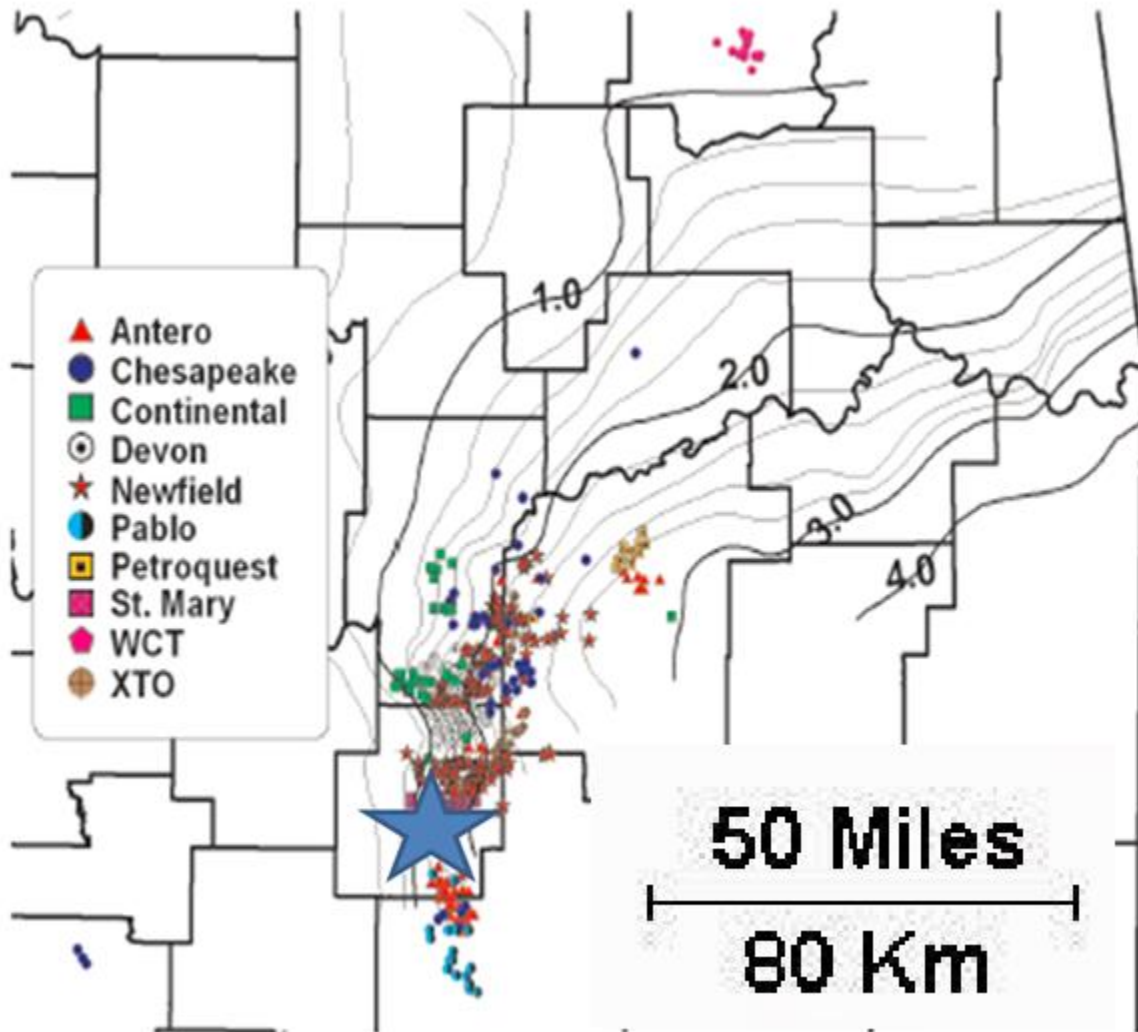


Figure 8. Isoreflectance vitrinite map of eastern Oklahoma indicating gradient change throughout the Arkoma Basin, overlain with the top 10 major operators 2004-2008; the blue star is the approximate location of the well (modified from Cardott, 2008).

2.4 - TOTAL ORGANIC CONTENT OF WOODFORD SHALE

Total organic content (TOC) is a measure of the amount of organic matter in a sample. It is calculated by taking the weight percentage of TOC from a sample, such as from the Woodford Shale, and comparing to the total rock weight. The TOC of Woodford Shale within the Arkoma Basin generally ranges between 1 to 10 wt% but can exceed 20 wt% in various areas (Houseknecht, 2014). The Woodford Shale within the Arkoma Basin is Kerogen type II (Cardott, 2013). Based on a study of the Woodford Shale by Comer (2008), the TOC can vary considerably within a county. From his study the Woodford Shale has TOC values ranging from 1-7 wt% (Figure 9).

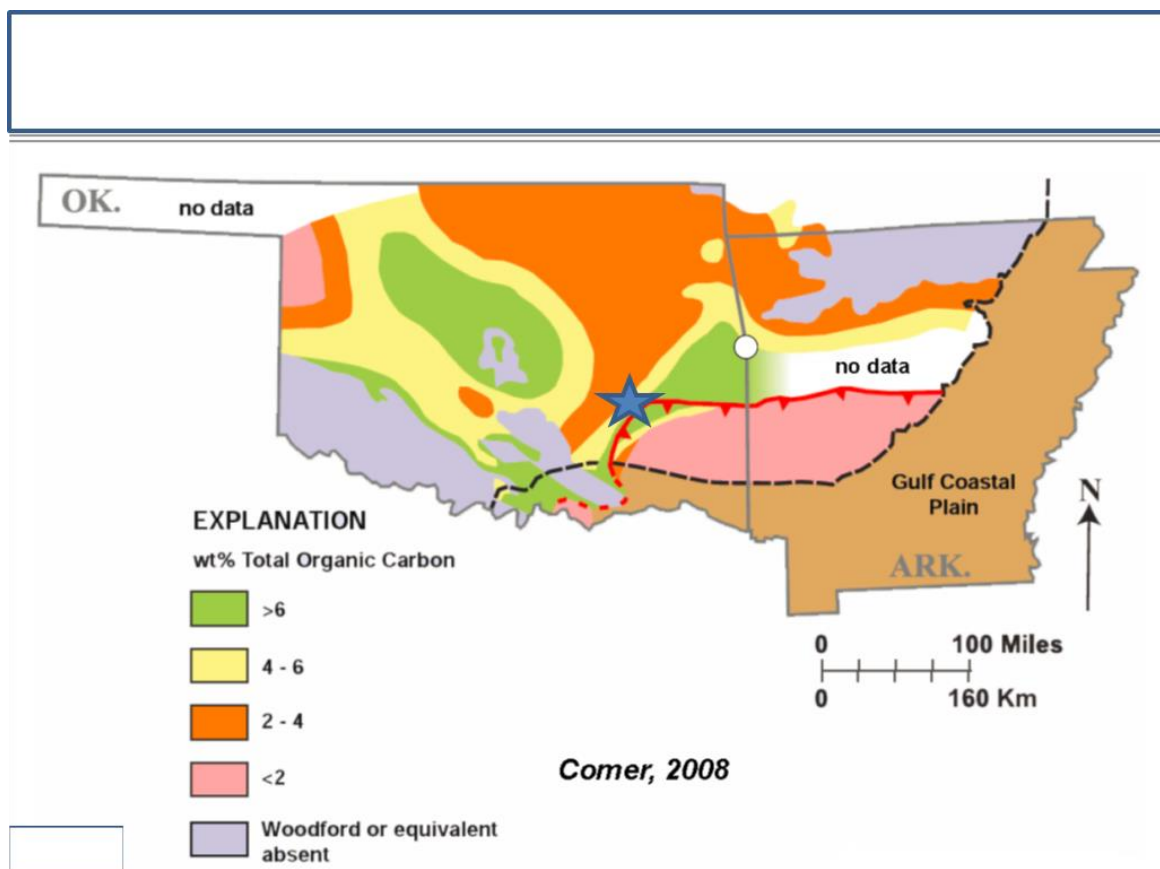


Figure 9. The wt% total organic carbon for Woodford Shale in Oklahoma and western Arkansas, the blue star is the approximate location of the well of this study (Comer, 2008). The black dotted line outlines the Coastal Plain. The red line with the triangles are to define Ouachita Thrust (Northcutt and Campbell, 1995).

The mineralogical composition of the Woodford Shale has been shown to control its brittleness (Caldwell, 2014), which is important for predicting the success rates of fracking the shale (Caldwell, 2014). The Middle Woodford, which is comprised of highly siliceous lithologies, has a significantly higher chance of success than clay-rich, more ductile mudrock shale facies (Caldwell, 2014). The most productive wells have a good compromise between high TOC and enough quartz content to be easily fractured.

Chapter 3 - HYPOTHESIS

The hypothesis is that the Woodford Shale is heterogeneous in both TOC and mineralogy across distances as small as a mile. This heterogeneity of the mineralogy and organic content can affect both the rock mechanics and hydrocarbon content, and should be measured when evaluating a well's potential (Caldwell, 2014; Wiley 2015; Turner et al., 2015a; McColloch, 2016). This hypothesis was tested using samples from the Pablo Carleigh 6H-32 well, which is a horizontal wellbore that remains primarily within the middle Woodford Shale for almost a mile. Based on this hypothesis and using the workflow described below, operators should be able to increase production of the well by optimizing areas to perforate and frack in the well.

Chapter 4 - METHODOLOGY

The methodology included the use of X-Ray Diffraction (XRD) to determine mineralogy, Handheld X-Ray Fluorescence (HHXRF) to determine whole-rock chemistry, and a muffle furnace to determine loss on ignition (LOI). LOI is an established proxy for TOC (McColloch, 2016). A type of normative mineralogy was calculated from a combination of XRD and HHXRF data, and brittleness (i.e. frackability) was estimated on the basis of the calculated mineralogy (Janssen, 2017).

Samples of the Woodford Shale were taken approximately every 30 feet in the Pablo-Carleigh 6H-32 well. This yielded more samples than could be realistically processed within the timeframe available, so to reduce the number only every other sample (60-foot intervals) was selected for analysis, resulting in approximately 75 samples included in this study.

Samples were powdered, using a mortar and pestle, to an estimated particle size of 4.0-3.5 ϕ . Powder was placed in powder caps for Handheld XRF, random powder receptacles for XRD, and crucibles for the loss on ignition analyses.

4.1 - Handheld X-Ray Fluorescence

The Bruker Handheld XRF (HHXRF) can analyze elements from Mg to U. Major and trace elements are analyzed separately, using different operating conditions.

For major element analysis, each sample was scanned three times with the HHXRF. This required the yellow filter be removed and the vacuum system used to remove the air between the HHXRF detector window and the detector. The power settings were 15kV and 25 μ A and an analysis time of 180 seconds per sample was used. For trace elements, each sample was again scanned three times. This required the use of the yellow filter, but did not require the vacuum system. The power settings were 40kV and 1.2 μ A on the HHXRF, with an analysis time of 60

seconds per sample. The raw data were processed using the S1PSRF program provided by the manufacturer. After every 5th sample, the standards (Bruker Duplex 2205 and RTC-W-220) were analyzed to ensure data quality.

4.2 – Bulk Powder X-Ray Diffraction

For bulk powder X-ray diffraction analysis, the material to be analyzed was finely ground and homogenized (Dutrow & Clark, 2016). Analyses were completed using the Panalytical Empyrean with the PIXcel 3D using a copper anode. Samples were analyzed from 2-65°2 θ with a step size of 0.007°2 θ . Generator settings were 20mA, 35 kV and scanning was continuous, taking a total of 20 minutes per scan.

The bulk powder XRD was used to determine which minerals were present in the samples. Random powder mounts were used; the resulting 2 θ and d-spacing of the peaks' measurements were used to determine which minerals the peaks represented. The data were normalized so the intensity ranges from 0 to 100. Minerals were identified from peak position using data from Moore and Reynolds (1997).

4.3 - Loss on Ignition (as a proxy for TOC)

Total organic carbon (TOC) was estimated using a proxy method of loss on ignition. The method is based on the observation of Dean (1974) that organic material begins to ignite at about 200° C and is completely ignited by approximately 550° C. Above this temperature, CO₂ is released as carbonate minerals are ignited (McColloch, 2016). Performing loss on ignition at 550° C on organic carbon is linear, see Figure 10 (Dean 1974).

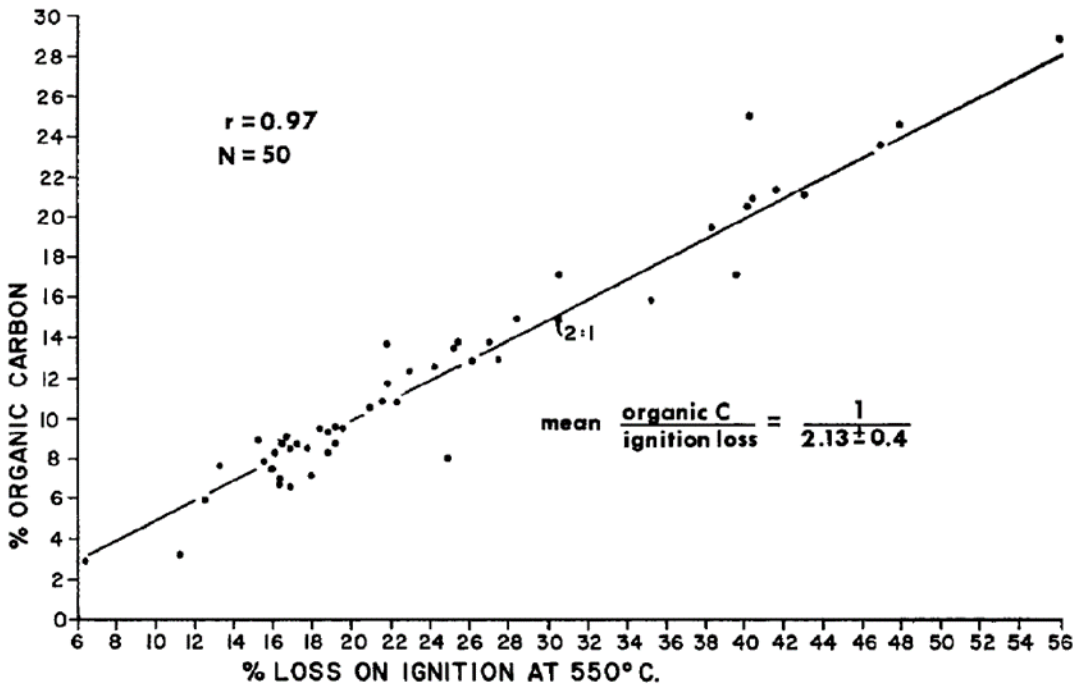


Figure 10. A scatter diagram of percent ignition loss at 550° C and percent organic carbon (modified from Dean, 1974).

The same powdered samples used in the HHXRF and XRD analyses were used for the LOI determination. Samples were emptied into the crucible, placed in the muffle furnace at 90 ° C for one hour to remove moisture from the samples. Samples were cooled to room temperature in a desiccator to prevent rehydration from humidity of the air. The samples were weighed, resulting in an initial dry weight. The samples were then placed in the muffle furnace and heated to 550 ° C for one hour. After cooling to room temperature, the samples were re-weighed. The difference from the weight compared to the initial dry weight approximates the total amount of organic carbon (TOC) in each sample (McColloch, 2016).

Chapter 5 - RESULTS

5.1 - HHXRF Results

Samples are listed in order of measured distance from the wellhead and were collected during the drilling of the well. The samples for this study were taken from the horizontal portion of the well. The table data is located within Appendix A for both the major and trace element HHXRF data.

Major element concentrations (wt%) determined by HHXRF are shown relative to distance along the well path in Figure 11. The large excursions in weight percent at ~7500 ft reflect the well path leaving the Woodford and crossing into the Hunton Limestone. The diagrams show that elements, such as Al, Si, and K, which are high in the shale, are much lower in the limestone. Surprisingly, Ca is lower in this part of the Hunton than in the Woodford, whereas Fe, S, and P are significantly elevated.

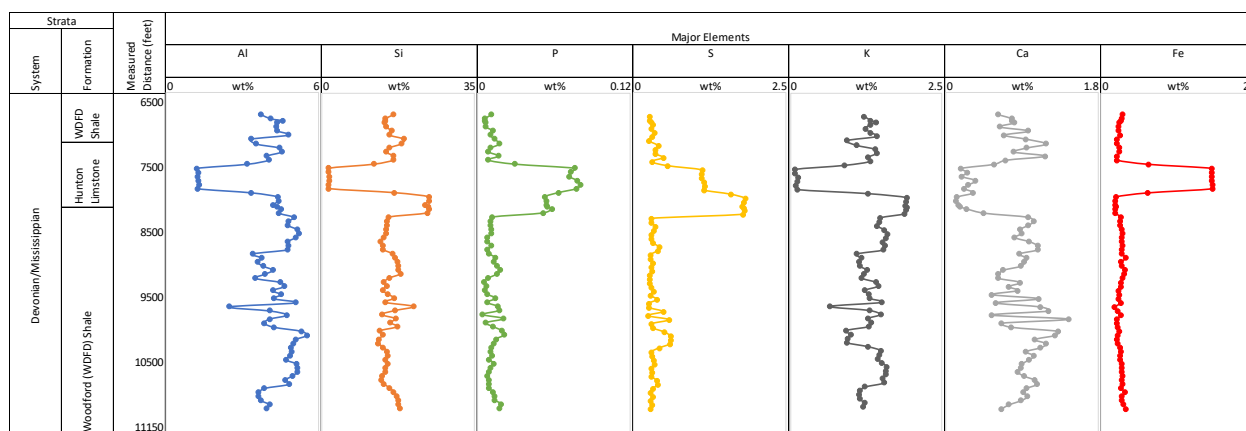


Figure 11. Major Elements

Trace element concentrations (ppm) determined by HHXRF are shown in Figure 12 relative to distance along the well path. Large shifts in Mo, V, Cr, and Mn concentrations are observed at the same position as the major element variations, i.e. where the well path crosses

from the Woodford to the Hunton (i.e. ca. 7,500 ft). In contrast, most other trace elements show no significant variation across this boundary

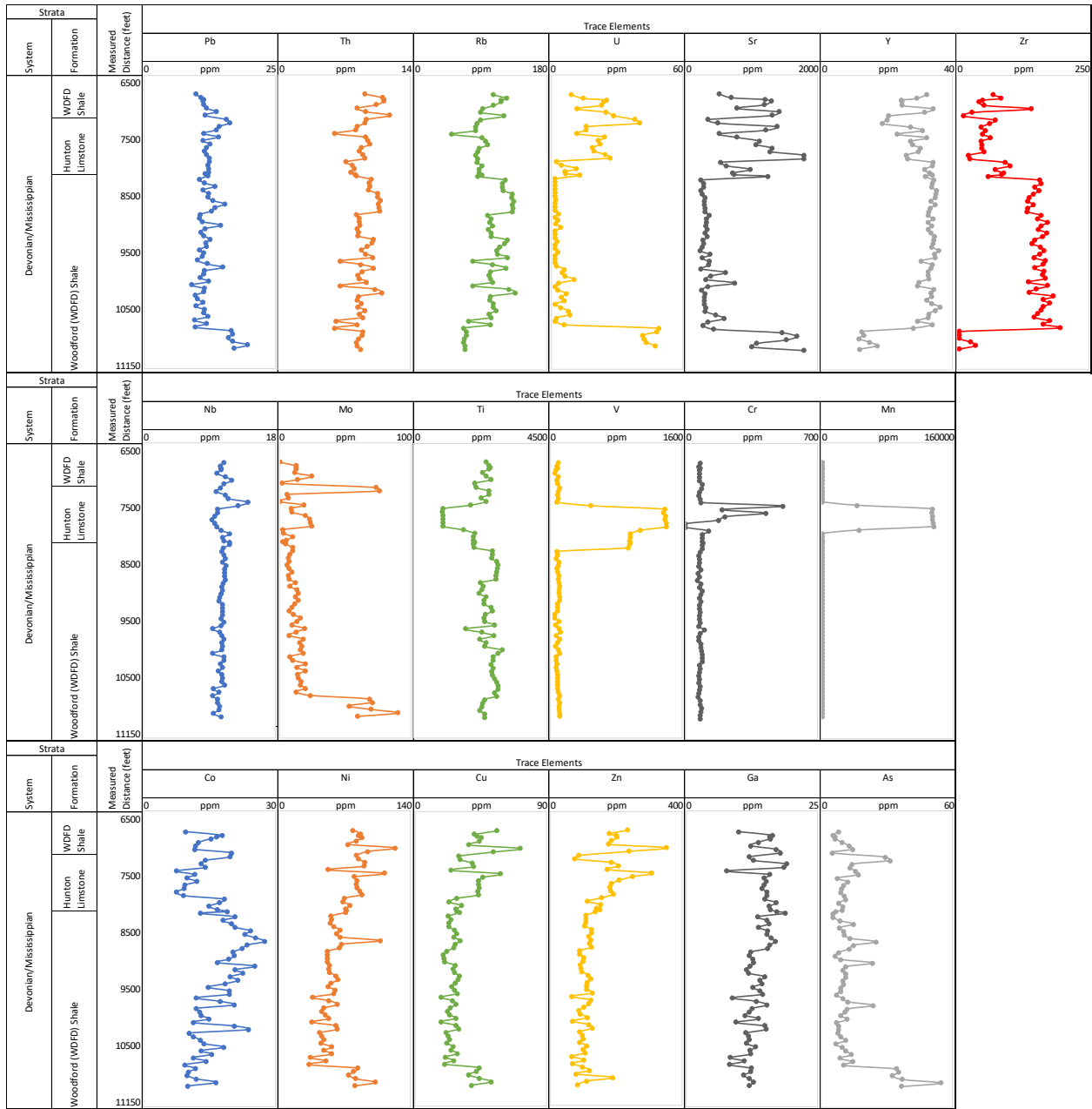


Figure 12. Trace Elements

5.2 – XRD Results

The XRD bulk powder diffractograms are used to determine mineralogy of the samples. Sample 6820 shown below is an example of the diffractograms acquired (Figure 13). The remaining bulk diffractograms are presented in Appendix B.

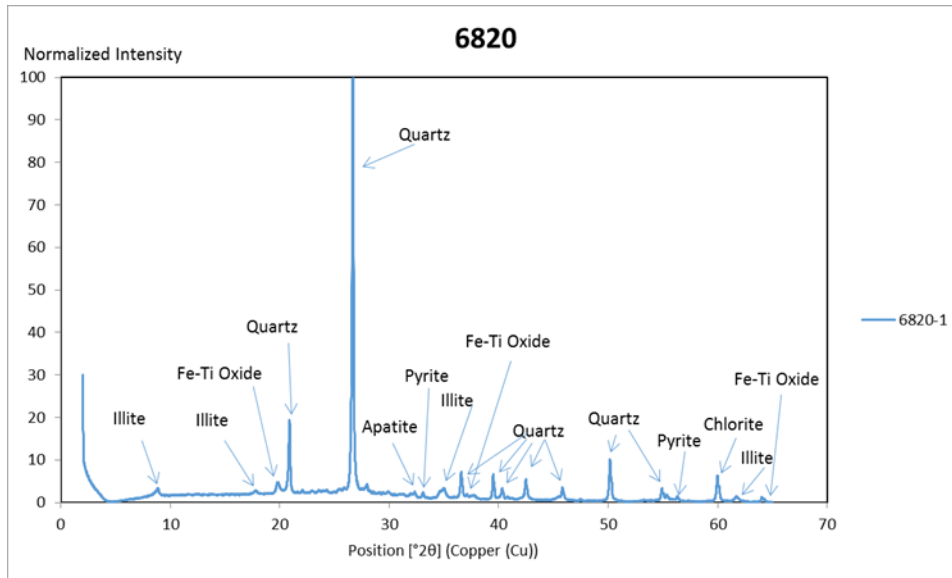


Figure 13. Bulk XRD diffractogram, sample 6820 example

The vertical axis, 0-100, is normalized intensity, calculated by dividing the intensity of each position by the intensity of the strongest peak in the scan. The horizontal axis is given in degrees 2θ . The measured peak positions were interpreted to determine the minerals present in each sample based on Moore and Reynolds (1997). Only six minerals are commonly identified from their characteristic peak positions: illite, pyrite, apatite, Fe-Ti oxides, dolomite, chlorite, and quartz, and these are annotated on each figure in Appendix B. Samples identified as Hunton Limestone show elevated abundances of Fe-Ti oxides and/or pyrite. Illite was the predominate clay mineral in all samples. Mixed-layer clay, such as smectite, was not identified in the samples, confirming the results of Janssen (2017).

The interpretation of mineral abundance is based on the peak intensity of the mineral at a given position and/or where the same mineral(s) peak at different positions throughout the sample. Table 1 identifies the abundance of minerals within the well path that were detected using the XRD. The legend for the table: “X” – minerals are minimally present, “XX” – minerals are common, “XXX” – minerals are abundant.

The table shows that the abundance of minerals changed throughout the well path. Illite is common in samples 6820–8870 and present elsewhere. Pyrite is abundant within the Hunton Limestone and directly following into the Woodford Shale up to sample 8270. Fe-Ti oxide was common at the beginning of the well path and diminishes to present at sample 8810. Apatite is present throughout the well path. Chlorite is common or abundant throughout the samples with the exception of samples 7850-8270. Dolomite was common for the samples prior to the Hunton Limestone where it is present until it becomes abundant at sample 10730. Quartz is abundant throughout the well path, except when the well path deviated into the Hunton. Note, that the apparent abundance of quartz based upon only XRD conflicts with the HHXRF as it shows a decrease in silicon, and the calculated amount of quartz. This is because the structural factor of quartz is so high as reflected by XRD peak intensity, particularly compared to the clay minerals. An analogous difference in XRD peak intensity is seen between chlorite and illite, because the structure factor of chlorite is higher than illite. These results emphasize the value in the calculated mineral percentages using the combination of XRD peak presence and HHXRF major element data.

Sample in ft	Minerals Identified from XRD diffractograms classified by interpretation						
	illite	pyrite	Fe-Ti oxide	apatite	chlorite	dolomite	quartz
6820	XX	XX	XX	X	XX	X	XXX
6880	XX	X	XX	X	XX	XX	XXX
6910	XX	X	XX	X	XX	XX	XXX
6940	XX	X	XXX	X	XX	XX	XXX
7000	XX	X	XX	X	XX	XX	XXX
7060	XX	X	XX	X	XX	XX	XXX
7120	XX	X	XX	X	XX	XX	XXX
7180	XX	X	XX	X	XX	XX	XXX
7250	XX	X	XX	X	XX	XX	XXX
7310	XX	X	XX	X	XX	XX	XXX
7370	XX	X	XX	X	XX	XX	XXX
7430	XX	X	XX	X	XX	XX	XXX
*7490	XX	XXX	XX	X	XXX	X	XXX
*7550	XX	XXX	XX	X	XXX	X	XXX
*7610	XX	XXX	XX	X	XX	X	XXX
*7670	XX	XXX	XX	X	XX	X	XXX
*7730	XX	XXX	XX	X	XX	X	XXX
*7790	XX	XXX	XX	X	XX	X	XXX
*7850	XX	XXX	XX	X	X	X	XXX
*7910	XX	XXX	XX	X	X	X	XXX
7970	XX	XXX	XX	X	X	X	XXX
8030	XX	XXX	XX	X	X	X	XXX
8090	XX	XXX	XX	X	X	X	XXX
8150	XX	XXX	XX	X	X	X	XXX
8180	XX	XXX	XX	X	X	X	XXX
8210	XX	XXX	XXX	X	X	X	XXX
8270	XX	XXX	XX	X	X	X	XXX
8330	XX	XX	XX	X	XX	X	XXX
8390	XX	XX	XX	X	XX	X	XXX
8450	XX	X	XX	X	XX	X	XXX
8510	XX	X	XX	X	XX	X	XXX
8570	XX	X	XX	X	XX	X	XXX
8630	XX	X	XX	X	XX	X	XXX
8690	XX	X	XX	X	XX	X	XXX
8750	XX	X	XX	X	XX	X	XXX
8810	XX	X	XX	X	XX	X	XXX
8870	X	X	X	X	XX	X	XXX
8930	X	X	X	X	XX	X	XXX
8990	X	X	X	X	XX	X	XXX
9050	X	X	X	X	XX	X	XXX
9110	X	X	X	X	XX	X	XXX
9170	X	X	X	X	XX	X	XXX
9230	X	X	X	X	XX	X	XXX
9290	X	X	X	X	XX	X	XXX
9350	X	X	X	X	XX	X	XXX
9410	X	X	X	X	XX	X	XXX
9470	X	X	X	X	XX	X	XXX
9530	X	X	X	X	XX	X	XXX
9590	X	X	X	X	XX	X	XXX
9650	X	X	X	X	XX	X	XXX
9710	X	X	X	X	XX	X	XXX
9770	X	X	X	X	XX	X	XXX
9830	X	X	X	X	XX	X	XXX
9890	X	X	X	X	XX	X	XXX
9950	X	X	X	X	XX	X	XXX
10010	X	X	X	X	XXX	X	XXX
10070	X	X	X	X	XX	X	XXX
10130	X	X	X	X	XX	X	XXX
10190	X	X	X	X	XX	X	XXX
10250	X	X	X	X	XX	X	XXX
10310	X	X	X	X	XX	X	XXX
10370	X	X	X	X	XX	X	XXX
10430	X	X	X	X	XX	X	XXX
10490	X	X	X	X	XX	X	XXX
10550	X	X	X	X	XX	X	XXX
10610	X	X	X	X	XX	X	XXX
10670	X	X	X	X	XX	X	XXX
10730	X	X	X	X	XX	XX	XXX
10790	X	X	X	X	XXX	XXX	XXX
10850	X	X	X	X	XX	XXX	XXX
10910	X	X	X	X	XX	XXX	XXX
10970	X	X	X	X	XX	XXX	XXX
11030	X	XXX	X	X	XX	XXX	XXX
11090	XXX	XXX	X	X	XX	XXX	XXX
11150	X	XXX	X	X	XX	XXX	XXX

Table 1. Mineral XRD interpretation of abundance. The legend for the table: X – minerals are minimally present to present, XX – minerals are common, XXX – minerals are abundant. The Hunton Limestone is indicated with an asterisk next to the sample number, otherwise the rest of the samples are identified as Woodford Shale.

5.3 – Loss on Ignition Results

Loss on ignition (LOI) was used to estimate TOC using the expression $(LOI) \cdot 0.84 - 1.1 = TOC$ proxy (McColloch, 2016); this method is based on the results of Dean (1974). The data shows that about 80% of the samples are around 5-15 wt% percent LOI and have 3-12 wt% percent organic carbon. The remaining samples are around 18-30 wt% percent LOI and have 15-23 wt% percent organic carbon with the exception of sample 7490 which has 56 wt% percent LOI and 47 wt% percent organic carbon.

Calculated TOC ranges between 4 wt% and 47 wt% (Table 2). The average calculated TOC for all samples is 9.3 ± 6.0 wt%, which is higher than the median which is 7.5 wt%.

TOC information	wt%
Average	9.32
Median	7.51
Standard Deviation	5.96
Min	3.96
Max	46.72

Table 2 - TOC information statistics.

Figure 14 shows the variation of the calculated TOC values along the well path. The data show higher TOC at the beginning of the well path before sample 7490 and then again towards the end of the well path starting around sample 10790. The data are presented in Appendix C.

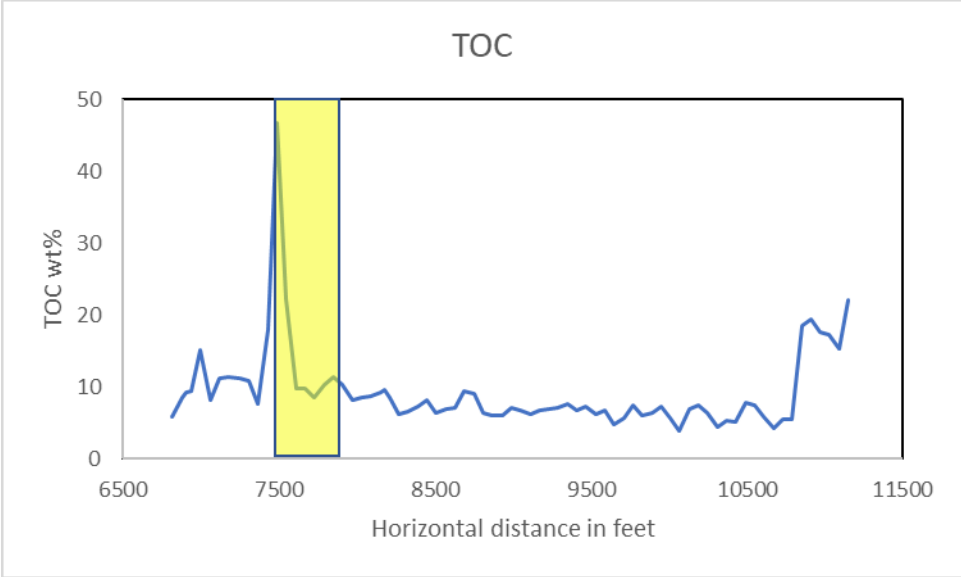


Figure 14. TOC across the well path, yellow is Hunton Limestone.

Chapter 6 - DISCUSSION

6.1 – Calculated Mineralogy

Estimating the mineralogy of shales from XRD data is particularly troublesome, given the extreme differences in structural characteristics of minerals such as quartz and clays (Totten et al., 2002). Combining the results of the XRD, which was used to determine the mineralogy, with the results of the HHXRF, which was used to determine the bulk composition, made it possible to model mineralogical proportions. The description of the calculation method and the calculated mineralogical data is in Appendix D. Figure 15 is the visual interruption of the calculated mineralogy results throughout the well path; the Hunton Limestone interval is excluded from this analysis, given that this unit is not the subject of this study. The general mineralogy remains similar throughout the well path, although some significant variations are observed (Fig. 15).

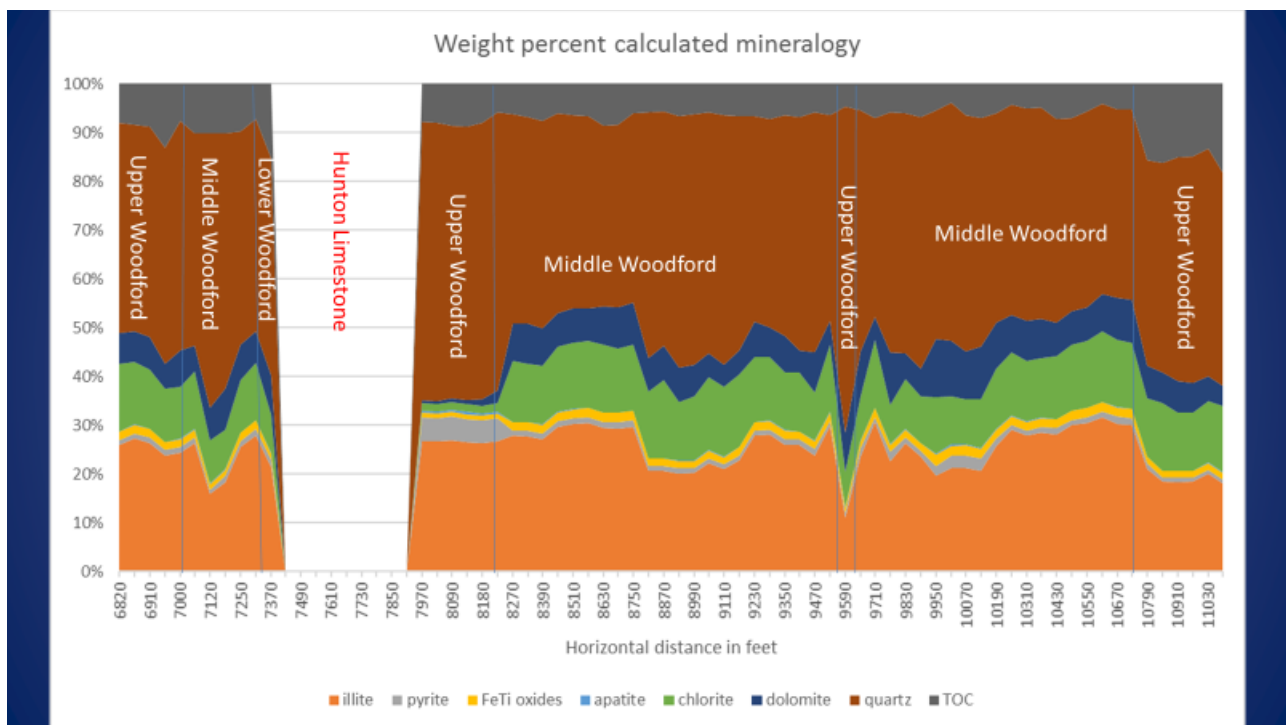


Figure 15. Wt% calculated mineralogy vs distance along the well path, with an interpretation based on the calculated mineralogy.

The well path does not remain within the same interval of the Woodford shale across its entire extent. This is first seen on the geosteering report (Figure 16), which is primarily based upon the gamma ray log. This stratigraphic variation is also apparent in the calculated mineralogic results of this study, as discussed below.

The data from the interval between 7910-8210ft along the well path is unique, because of the small amounts of chlorite and dolomite, the elevated levels of pyrite and the large amounts of quartz; the geosteering interpretation shows this section to be near the boundary of the Upper and Middle Woodford Shale (Figure 16). We interpret this section as being Upper Woodford Shale (or near enough to the boundary to be distinctly different than Middle Woodford). This is supported by the description of the Upper Woodford Shale indicating elevated quartz can be present (Comer, 2008; Lambert, 1993). The range of the calculated mineralogy for this section is illite 26-28wt%, pyrite 5wt%, Fe-Ti oxides 1wt%, apatite <1wt%, chlorite 1-2wt%, dolomite 1-3wt%, and quartz 57wt%.

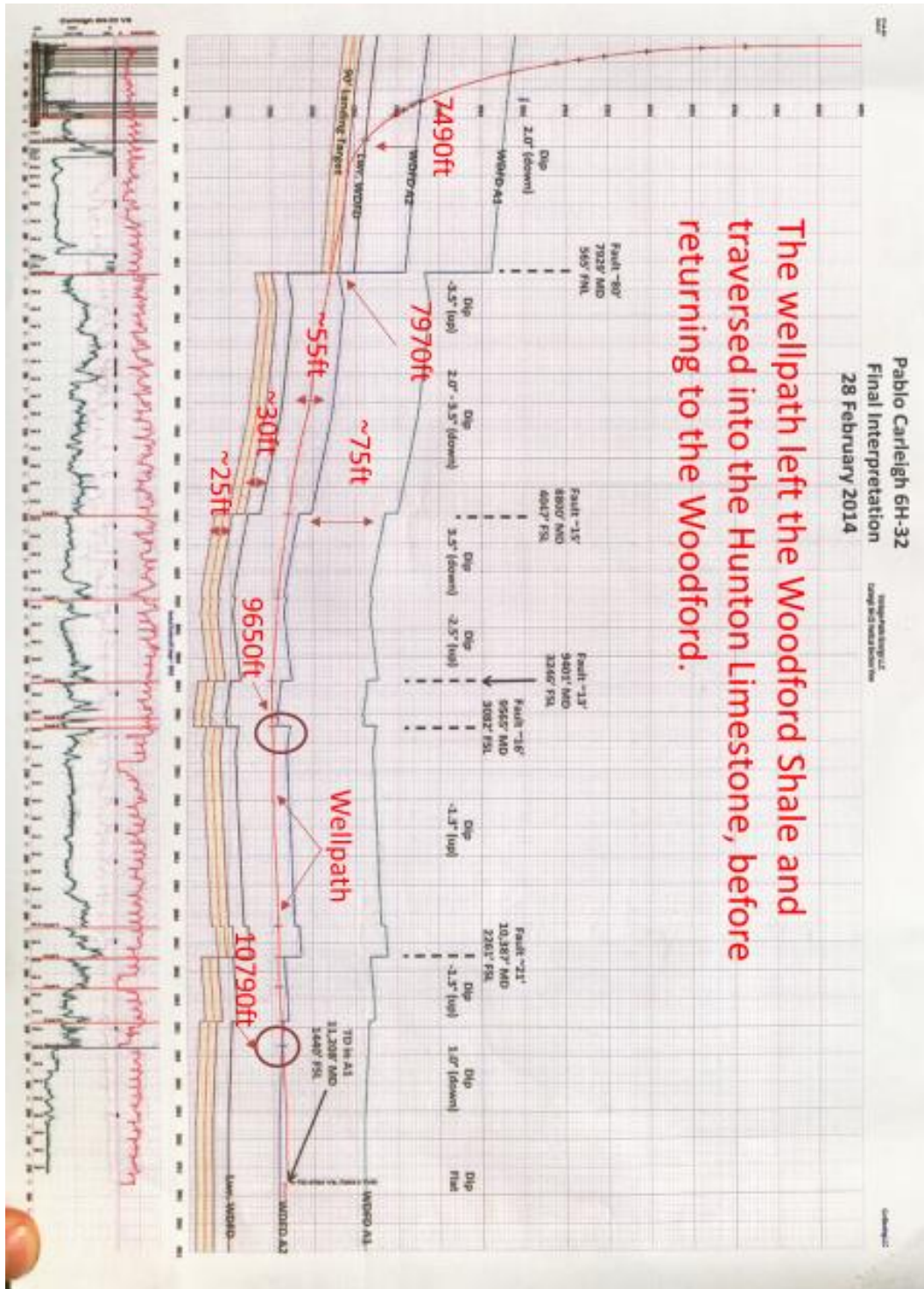
The data from the interval between 8210-10710 ft has a calculated mineralogy consistent with the Middle Woodford Shale, with one exception at 9650 ft, which is discussed below. The range of the calculated mineralogy for this section, excluding 9650, is illite 20-31wt%, pyrite 1-4wt%, Fe-Ti oxides 1-2wt%, apatite 0.5wt%, chlorite 7-15wt%, dolomite, 4-12wt%, and quartz 37-51wt%.

The individual sample at 9650 ft measured distance along the horizontal well path is speculated to also be from the Upper Woodford Shale based on the same reasoning as before. The geosteering interpretation again shows this sample near the boundary between Upper and

Lower Woodford, and the calculated mineralogy is consistent with samples from the Upper Woodford Shale. The TOC wt% is lower for this single sample than compared to the other samples from 10790-11150ft. The calculated mineralogy for sample 9650 is illite 11wt%, pyrite 1wt%, Fe-Ti oxides 1wt%, apatite <1wt%, chlorite 7wt%, dolomite 8wt% and quartz 67wt%.

The data for the interval between 10790-11150 ft along the well path is interpreted as Upper Woodford Shale based on the geosteering interpretation and is consistent with our calculated mineralogy. The range of the calculated mineralogy for this section is illite 18-21wt%, pyrite 1wt%, Fe-Ti oxides 1-2wt%, apatite <1wt%, chlorite 12-14wt%, dolomite 4-7wt%, and quartz 42-47wt%.

The calculated mineralogy shows lateral variations in samples from confirmed Middle Woodford Shale. This variation could be due to subtle changes of stratigraphic position within the Middle Woodford Shale. Alternatively, the variations could be from lateral variations within the same stratigraphic horizon. The geosteering interpretation based primarily upon gamma ray intensity collected during drilling is not sensitive enough to determine the exact cause of the mineral variability.



The wellpath left the Woodford Shale and traversed into the Hunton Limestone, before returning to the Woodford.

Pablo Carleigh 6H-32
Final Interpretation
28 February 2014

Figure 16. Well path of Pablo Carleigh 6H-32. The abbreviations are as follows: FSL, Feet South Line; FNL, Feet North Line, these are used mainly to ensure operators are not taking resources they did not lease or own beyond their line, WDFD A1, Upper Woodford Shale; WDFD A2, Middle Woodford Shale; Lwr. WDFD, Lower Woodford Shale; MD, Measured Distance. The red line at the bottom is the resistivity curve and the green line at the bottom is the gamma ray.

6.2 - Mineral Brittleness Index

The Mineral Brittleness Index (MBI) based on the Wang and Gale (2009) formula (Figure 17) utilizes the results from the calculated mineralogy and the calculated TOC which estimates the brittleness of the sample. The MBI indicates the breakability of the shale, which is useful in understanding how fragile the shale is throughout the well path.

Calculated MBI for all samples are presented in Appendix D; the range of calculated values is 41 to 76.5 (Table 3). Average MBI for all Woodford Shale samples is 54.5 ± 6.0 , which is higher than the median of 53.4. The variation in MBI across the horizontal distance of the well path, excluding the Hunton Limestone, is show in Figure 18 and tabled in Appendix D. The MBI vs calculated modal proportion of quartz shows a positive correlation (Figure 19).

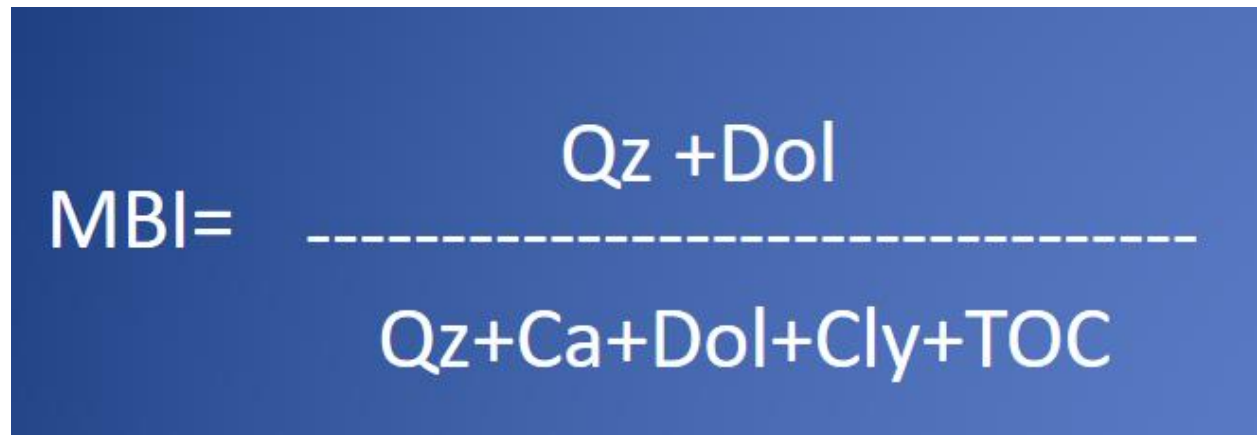
The image shows the Mineral Brittleness Index (MBI) formula on a blue background. The formula is presented as a fraction. The numerator is 'Qz + Dol' and the denominator is 'Qz + Ca + Dol + Cly + TOC'. A dashed horizontal line separates the numerator and denominator. To the left of the fraction, the text 'MBI =' is written.
$$\text{MBI} = \frac{\text{Qz} + \text{Dol}}{\text{Qz} + \text{Ca} + \text{Dol} + \text{Cly} + \text{TOC}}$$

Figure 17. Mineral Brittleness Index formula used from (Wang and Gale, 2009)

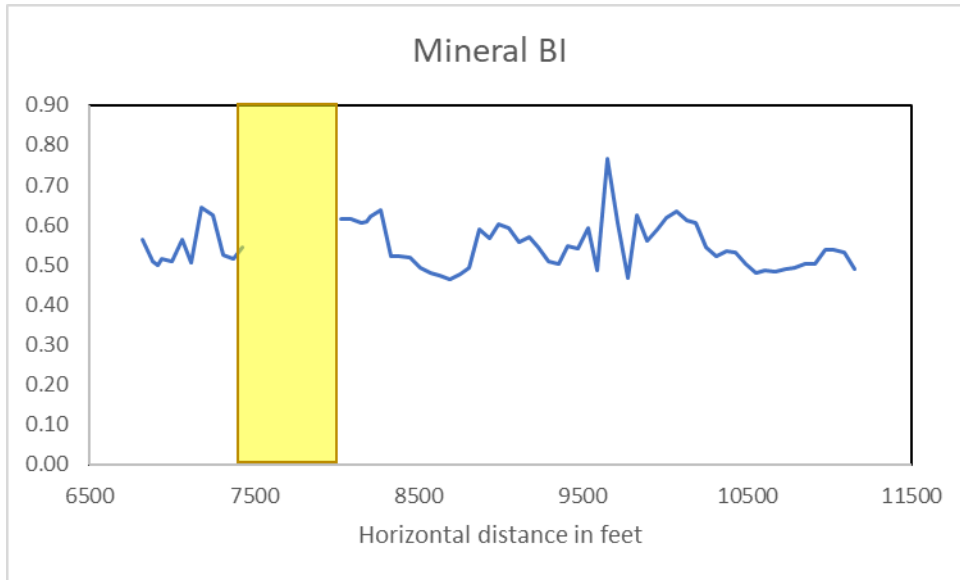


Figure 18. Mineral Brittleness Index as per Wang and Gale (2009) across the well path, excluding the Hunton Limestone

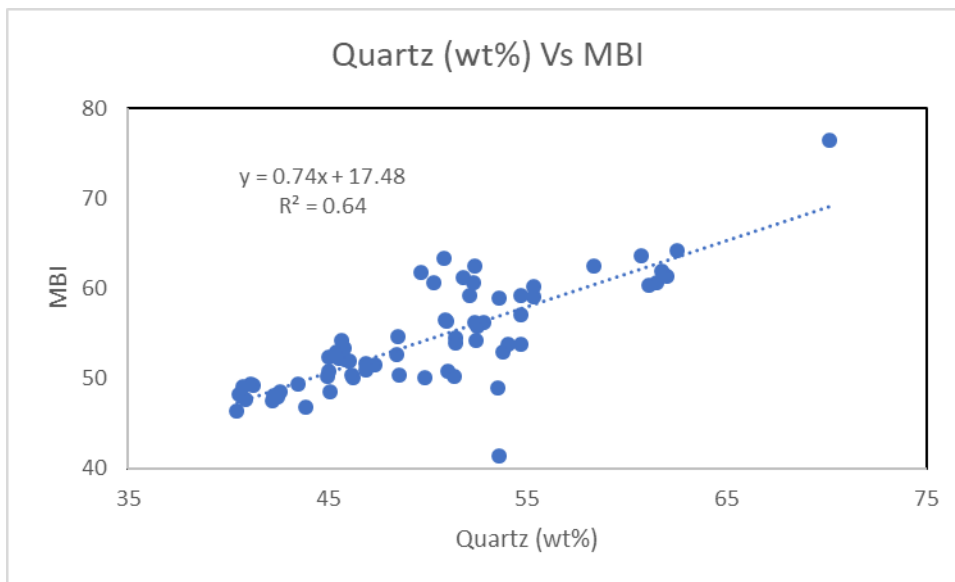


Figure 19. Samples from the Woodford Shale well path comparing Quartz (wt%) versus MBI variation.

MBI Information	
Average	54.49
Median	53.38
Standard Deviation	5.95
Min	41.41
Max	76.45

Table 3. MBI Statistical Information of the Woodford Shale

6.3 - Frack Gradient and Mineral Brittleness Index

Frack Gradient is a factor to determine formation fracturing pressure as a function of well depth in units of psi/ft (pounds per square inch/foot) (Schlumberger.com, 2017). The “Top of 4’ gun” is where Pablo Energy performed the frack at each of three locations for each stage. The samples used for this comparison were the ones closest to the frack locations. The first stage starts at the end of the well path and moves back towards the wellhead as they perforate. While most stages have three samples for MBI, stage 10 has two samples and stage 12 has only one sample (Table 4). Based on distances, stages 1-3 and 12 belong to the Upper Woodford Shale, whereas stages 4-11 belong to the Middle Woodford Shale.

Stage	Top of 4' gun			frack gradient	Samples used					Averaged MBI
1	11120	11025	10942	0.66	11090	11030	10970			0.54
2	10842	10752	10665	0.84	10790	10730	10670			0.49
3	10563	10474	10385	0.83	10550	10490	10430			0.50
4	10285	10188	10106	0.79	10250	10190	10130			0.59
5	10006	9917	9828	0.76	9950	9890	9830			0.59
6	9723	9638	9549	0.80	9710	9650	9590			0.62
7	9449	9360	9271	0.76	9410	9350	9290			0.52
8	9171	9082	8992	0.74	9170	9110	9050			0.57
9	8892	8803	8717	0.73	8870	8810	8750			0.52
10	8614	8525	8435	0.75	8570	8510				0.49
11	8335	8250	8150	0.78	8330	8270	8210	8180	8150	0.60
12	8083	8039	7980	0.79	8030					0.62

Table 4. Stage and perforating information along with a list of samples used to generate MBI; modified from Pablo Carleigh (2014).

Figure 20 shows a plot of frack gradient vs. MBI for the twelve stages where the fracking occurred. The red dots show the results for fracking of the Upper Woodford Shale whereas the blue dots show the results for Middle Woodford Shale. Collectively, the dataset shows no correlation between Frack Gradient and MBI.

However, samples from just the Middle Woodford Shale show a correlation between the Frack Gradient and MBI (Figure 21). The MBI, therefore, is a reasonable predictor of frack gradient within the Middle Woodford Shale, which is the primary target. The MBI can be calculated after drilling, and used to help plan perforation locations to optimize frack gradient. This could also be combined with TOC values to increase the economic potential of the well.

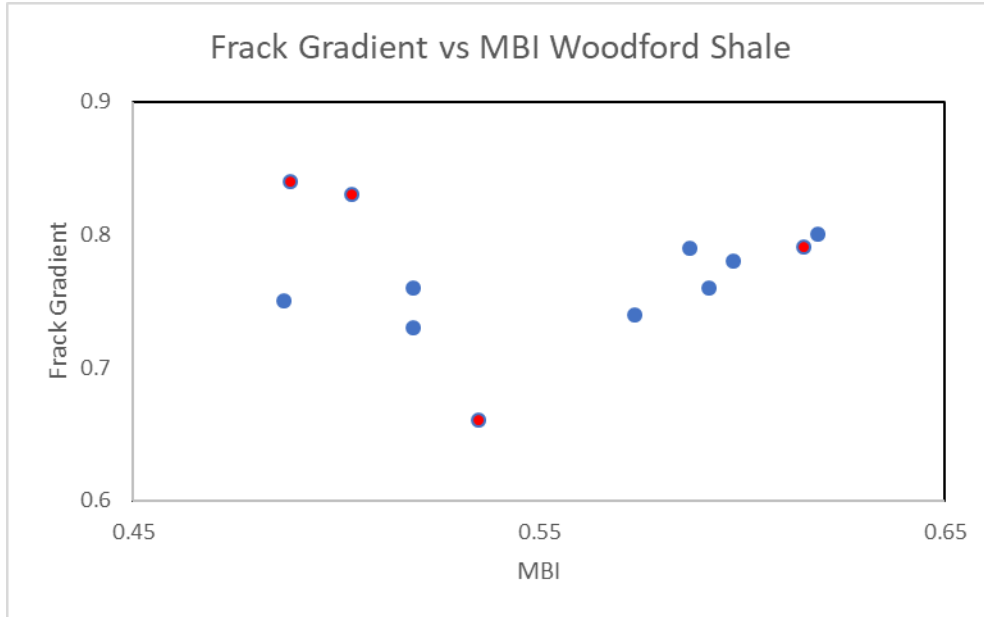


Figure 20. MBI versus frack gradient. Upper Woodford Shale in red and Middle Woodford Shale in blue

The reasons for the poor correlation between Frack Gradient and MBI could stem from any of the following reasons: limited number of perforation stages, uncertainties associated with the calculated mineralogy, uncertainties associated with the calculated MBI, sample locations and perforation locations are different, and faults within the well path. Alternatively, there could exist separate relations within each subgroup of the Woodford Shale.

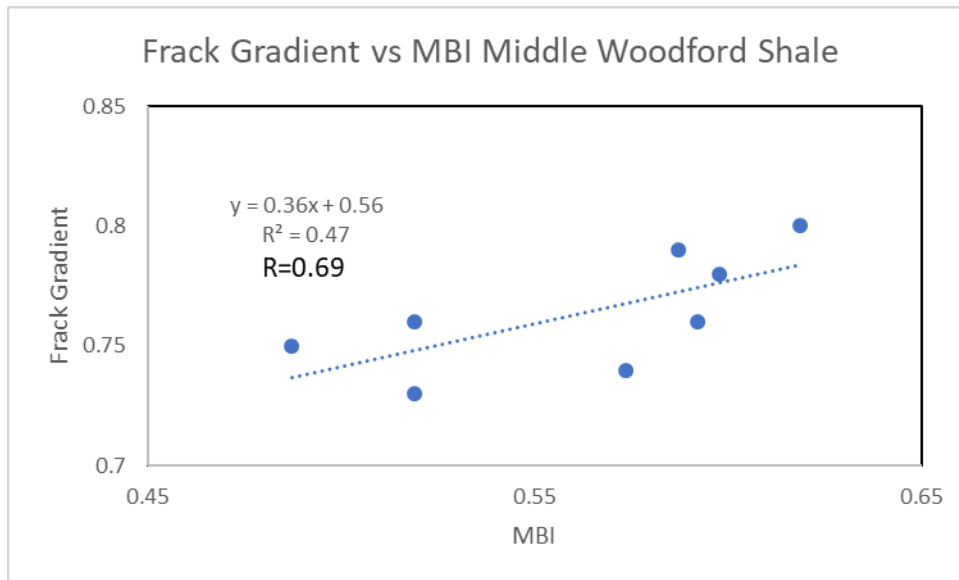


Figure 21. The use of Middle Woodford Shale samples MBI versus frack gradient correlate.

In summary, the calculated mineralogy is useful for identifying different subsections of the Woodford Shale and is also useful in calculating the MBI (Wang and Gale, 2009), which is a good predictor of frac gradient in the Middle Woodford Shale. It is not known why the other subgroups of the Woodford do not follow this association.

Chapter 7 - CONCLUSION

This study provides insights from investigating the variations of mineralogical properties, organic matter content, and elemental composition from samples taken from a horizontal well within the Upper/Middle Woodford Shale.

The calculated mineralogy was able to distinguish between Middle and Upper Woodford Shale. The calculated mineralogy is based on the mineralogy identified on the basis of XRD data and elemental concentrations determined by HHXRF. The calculated mineralogy is consistent with the geosteering interpretation of where the well path, and may be more sensitive to boundaries between the Upper and Middle Woodford Shale than the gamma ray log alone. Loss on ignition was determined as per Dean (1974) and McColloch (2016).

Trace element variations were not observed to correlate with other well properties, and are not as useful in predicting organic content as previous studies proposed. Their variation across the well path was not systematic.

The MBI was calculated using the Wang and Gale (2009) formula, using the calculated mineralogy and modeled TOC. Frack Gradient versus MBI shows correlation for the samples that are within the Middle Woodford Shale. The Middle Woodford is the target productive zone, therefore, predicting fracking potential based on calculated MBI could lead to better perforation and fracking designs.

References

- Amsden, T.W., 1975, Hunton Group (Late Ordovician, Silurian, and Early Devonian) in the Anadarko Basin of Oklahoma. Oklahoma Geological Survey Bull. 121, 214pp.
- Andrews, R.D., 2009, Production decline curves and payout thresholds of horizontal Woodford wells in the Arkoma Basin, Oklahoma (part 1): Oklahoma City Geological Society, Shale Shaker, v. 60, p. 103-112.
- Blakey, Ron., 2016, Regional Paleogeography. Northern Arizona University, Flagstaff Arizona. <http://jan.ucc.nau.edu/rcb7/nam.html> Accessed 02 November, 2016.
- Boyd, Dan T., 2006, Oklahoma 2006 Drilling Activity. Oklahoma Geological Survey. Shale Shaker May-June 2007, Shale Shaker, 199-208.
- Brewer, J. A., R. Good, J. E. Ouver, L. D. Brown, and S. Kaufman, 1983, COCORP Profiling Across the Southern Oklahoma Aulacogen: Overthrusting of the Wichita Mountains and Compression within the Anadarko Basin: Geology, v. 11, p. 109-114.
- Caldwell, C., 2014, Anadarko Woodford Shale: How to Tie a Shoe. Oklahoma City, Oklahoma., AAPG Search and Discovery Article #80408.
- Cardott, B. J., & Lambert, M. W., 1985, Thermal Maturation by Vitrinite Reflectance of Woodford Shale, Anadarko Basin, Oklahoma. *AAPG Bulletin*, v.71, 898-899.
- Cardott, B.J., 2008, Thermal Maturity of the Woodford Shale in Oklahoma Applied to the Gas-Shale Play.
- Cardott, B. J., 2012, Thermal Maturity of Woodford Shale Gas and Oil Plays, Oklahoma, USA: International Journal of Coal Geology, v. 103, p. 109–119.

Cardott, B.J., 2013, Determining the Thermal Maturity Level at Which Oil Can Be Economically Produced in the Woodford Shale. Oklahoma Geological Survey. Woodford Oil Congress 2014.

Comer, J. 2008, Arkoma Basin Gas Shales – OGS, USGS [ogs.ou.edu/docs/.../OGS-workshop-arkoma_2009-USGS5_shale_gas_resources.pdf](https://www.ogs.ou.edu/docs/.../OGS-workshop-arkoma_2009-USGS5_shale_gas_resources.pdf)

Dutrow, B., Clark C. 2016, Geochemical Instrumentation and Analysis. Louisiana State University and Eastern Michigan University.

The Energy Information Administration: Review of Emerging Resources: U.S. Shale Gas and Shale Oil Plays, 2011. Accessed 6 December 2017.

<https://www.eia.gov/analysis/studies/usshalegas/>

The Energy Information Administration: Frequently Asked Questions:

<https://www.eia.gov/tools/faqs/faq.php?id=46&t=8>

<https://www.eia.gov/tools/faqs/faq.php?id=907&t=8>

Garner, D. L., and D. L. Turcotte, 1984, The Thermal and Mechanical Evolution of the Anadarko basin: Tectonophysics, v. 107, p. 1-24.

Ham, W. E., 1964. Basement Rocks and Structural Evolution of Southern Oklahoma. Rocky Mountain Association of Geologist, v. 1 p. 89.

Hanson, Richard E.; Puckett Jr., Robert E.; Keller, Randy G.; Brueseke, Matthew E.; Bulen, Casey L.; Mertzman, Stanley A.; Finegan, Shane A.; McCleery, David A. (1 August 2013). "Intraplate magmatism related to opening of the southern Iapetus Ocean; Cambrian Wichita igneous province in the Southern Oklahoma rift zone". *Lithos*. 174: 57–70. doi:10.1016/j.lithos.2012.06.003.

Janssen, K. W. 2017. A study of the effects of organic matter on illitization in the Woodford Shale, Oklahoma and Kansas. Kansas State University, Department of Geology.

- Keller, G. R., E. G. Lidiak, W. J. Hinze, and L. W. Braile, 1983, The Role of Rifting in the Tectonic Development of the Midcontinent, U.S.A.: *Tectonophysics*, v. 94, p. 391-412.
- Kirkland, D. W., R. E. Denison, D. M. Summers, and J. R. Gormly, 1992, Geology and Organic Geochemistry of the Woodford Shale in the Criner Hills and Western Arbuckle Mountains, Oklahoma, in K. S. Johnson and B. J. Cardott, eds., *Source Rocks in the Southern Midcontinent*, Oklahoma Geological Survey, Circular 93, p. 38–69.
- Lambert, M.W., 1990, Internal Stratigraphy of the Chattanooga Shale in Kansas and Oklahoma, in Johnson, K.S. and B.J. Cardott (eds.) *Source Rocks in the Southern Midcontinent*, 1990 Symposium: Oklahoma Geological Society Circular 93, 94-103.
- Lambert, M.W., 1993, Internal Stratigraphy and Organic Facies of the Devonian-Mississippian Chattanooga (Woodford) Shale in Oklahoma and Kansas, *in* B.J. Katz and L.M. Pratt, eds., *Source Rocks in a Sequence Stratigraphic Framework: AAPG Studies in Geology* 37, p. 163-176.
- Lee, W., 1940, *Subsurface Mississippian Rocks of Kansas*: Kansas Geological Survey Bulletin 33, 114 p.
- Moore, D. M. and Reynolds, R. C., 1997, *X-Ray Diffraction and the Identification and Analysis of Clay Minerals*. Oxford University Press, New York.
- Northcutt, R. A. and Campbell, J. A., 1995, *Geological Provinces of Oklahoma. The Shale Shaker*.
- Monroe, J. S., and Reed W., *The Changing Earth: Exploring Geology and Evolution*, 2nd ed. Belmont: West Publishing Company, 1997. ISBN 0-314-09577-2 (pp. 539–44)
- Oklahoma Geological Survey. Accessed 21 September 2016.
<http://www.okgenweb.org/okprojects/coal/coal-1n-10e.gif>
<http://www.okgenweb.org/okprojects/xref/help/northeast-sw-links.htm>

- Portas, R., 2009, Characterization and origin of fracture patterns in the Woodford Shale in southeastern Oklahoma for application to exploration and development: M.S. thesis, University of Oklahoma, Norman, Oklahoma, 113 p.
- Potter, P., Maynard, J., and Pryor, W., 1980, Sedimentology of shale: Springer-Verlag, New York, 306 p.
- Rowe, H. and Hughes, N., 2010, Strategy for Developing and Calibrating Shale and Mudstone Chemostratigraphies Using Hand-Held X-ray Fluorescence Units, AAPG Annual Convention and Exhibition, New Orleans, Louisiana, April 11-14, 2010.
- Schlumberger Oilfield Glossary - fracture gradient. Accessed 01 March 2018.
http://www.glossary.oilfield.slb.com/Terms/f/fracture_gradient.aspx
- Totten, M. W., Blatt H., 1993, Alterations in the Non-Clay-Mineral Fraction of Pelitic Rocks Across the Diagenetic to Low-Grade Metamorphic Transition, Ouachita Mountains, Oklahoma and Arkansas, *Journal of Sedimentary Petrology*, Vol. 63 (1993)No. 5. (September), Pages 899-908.
- Totten, M.W., and Hanan, M. A., 1998, The Accessory Mineral Fraction of Mudrocks and its Significance for Whole-rock Trace-element Geochemistry: in Schieber, J., Zimmerle, W., and Sethi, P., eds., *Shales and Mudstones: Volume I: Petrography, Petrophysics, Geochemistry and Economic Geology*; Publisher: Schweizerbart, Stuttgart/Germany, p. 35-53.
- Totten, M.W., Hanan, M.A., and Weaver, B.L., 2000, Beyond Whole-rock Geochemistry of Shales: The Importance of Assessing Mineralogic Controls For Revealing Tectonic Discriminants of Multiple Sediment Sources For The Ouachita Mountain Flysch Deposits: *Geological Society of America Bulletin*, v. 112, p. 1012-1022.

- Totten, M.W., Hill, Tyler. and Lambert, M., 2011, Potential Source Rocks in the Western Kansas Petroleum Province. AAPG Search and Discovery Article #90133 Mid-Continent Section Meeting, Oklahoma City, Oklahoma, 1-4 October 2011.
- Tribovillard, N., Algeo, T.J., Lyons, T., Riboulleau, A., 2006, Trace metals as paleoredox and paleoproductivity proxies: an update. *Chem. Geol.* 232, 12e32.
- Tribovillard, N., Hatem, E., Averbuch, O., Barbecot, F., Bout-Roumazielles, V., Trentesaux, A. 2015, Iron availability as a dominant control on the primary composition and diagenetic overprint of organic-matter-rich rocks. *Chemical Geology*, 401, 67-82.
- Turner, B. Becerra-Rondon, D. Slatt, R. 2015a, How Variable Can Shales Be? Lessons of Mudrock Heterogeneity. University of Oklahoma. Search and Discovery Article.
- Turner, B. W., Tréanton, Jessica A., Slatt, R. M., 2015b, The Use of Chemostratigraphy to Refine Ambiguous Sequence Stratigraphic Correlations in Marine Shales: An Example from the Woodford Shale, Oklahoma. ConocoPhillips School of Geology and Geophysics, University of Oklahoma.
- Turner, B., Molinares-Blanco, C. E., Slatt, R., 2015c, Chemostratigraphic, palynostratigraphic, and Sequence Stratigraphic Analysis of the Woodford Shale, Wyche Farm Quarry, Pontotoc County, Oklahoma. *Interpretation: a Journal of Subsurface Characterization*.
- U.S. Department of Energy, Morgantown Energy Technology Center, 1981, Evaluation of Devonian shale potential in (New York: DOE/METC 118) (Pennsylvania: DOE/METC-119) (West Virginia: DOE/METC-120, available from NTIS) (Eastern Kentucky/Tennessee:DOE/METC-121) (Ohio: DOE/METC-122) (the Michigan basin:DOE/METC-123) (the Illinois basin: DOE/ METC-124): prepared for publication by Tetra Tech, Columbus, Ohio.

- Wall, M., 2015, An Oil-Source Rock Correlation Examining the Potential Of The Chattanooga Shale as a Source Rock for Oil Within the Spivey-Grabs-Basil Field, Kingman and Harper Counties, Kansas. Department of Geology, Kansas State University. Manhattan, Kansas.
- Walper, J. L., 1976, The Geotectonic Evolution of the Wichita Aulacogen, Oklahoma, *in* G. E. Henry, ed. Basins of the Southwest, Phase 2: North Texas Geological Society, p. 192-211.
- Walper, J.L., 1977, Paleozoic Tectonics of the Southern Margin of North America: Gulf Coast Association of Geological Societies Transactions, v. 27, p. 230-241.
- Wiley, Tyler J. 2015, Handheld XRF As a Proxy for Onsite Evaluation of Unconventional Targets: An Investigation of the Woodford Shale, Anadarko Basin, Oklahoma. Department of Geology, Kansas State University. Manhattan, Kansas.
- Zhang, J., Turner, B., Slatt, R., 2017, XRF Chemostratigraphy for Characterizing Shale Reservoir along a Horizontal Well Track. AAPG Search and Discovery Article #41993.
- USGS Article - The Public Land Survey System (PLSS) Accessed 2 December, 2017.
https://nationalmap.gov/small_scale/a_plss.html

Appendix A - HHXRF Table Concentrations

This Appendix A is here to create a centralized location of where the table concentrations are located that were not used within the main body of the texts. The tables provide precision information using RTC-W-220 and Bruker Duplex 2205 for both the majors and minors. The entire measured samples are from the start measured distance 6820 feet to the finish 11150 feet of the well path.

Major HHXRF Elemental Concentrations

Wt% of Major Elements							
Sample	Al	Si	P	S	K	Ca	Fe
6820	3.73	18.78	0.01	0.33	1.46	0.67	4.02
6880	4.12	16.59	0.01	0.32	1.59	0.86	3.86
6910	4.59	16.67	0.01	0.35	1.70	0.85	3.68
6940	4.36	16.29	0.01	0.38	1.59	0.89	3.46
7000	4.33	16.76	0.01	0.36	1.49	0.69	3.26
7060	4.38	18.33	0.01	0.42	1.59	1.08	3.31
7120	4.83	17.63	0.01	0.37	1.72	0.75	3.58
7180	3.33	21.47	0.02	0.31	1.13	1.04	2.92
7250	3.52	20.76	0.02	0.49	1.31	1.31	2.91
7310	4.46	17.62	0.01	0.44	1.67	1.05	3.41
7370	4.55	16.81	0.01	0.43	1.72	0.88	3.45
7430	3.94	18.76	0.02	0.60	1.54	1.30	2.96
7490	4.03	18.74	0.01	0.37	1.59	0.77	3.02
7550	3.17	13.63	0.04	0.68	1.07	0.62	9.17
7610	1.17	1.73	0.10	1.35	0.09	0.18	21.79
7670	1.22	1.79	0.09	1.35	0.09	0.27	21.74
7730	1.20	1.86	0.09	1.35	0.15	0.18	21.73
7790	1.25	1.96	0.10	1.39	0.13	0.37	21.80
7850	1.26	1.82	0.10	1.41	0.10	0.28	21.91
7910	1.21	1.83	0.10	1.39	0.13	0.22	21.93
7970	3.34	18.94	0.08	1.91	1.53	0.34	9.10
8030	4.39	28.00	0.07	2.20	2.31	0.13	2.74
8090	4.41	27.95	0.07	2.17	2.30	0.11	2.70
8150	4.20	26.92	0.07	2.14	2.27	0.14	2.69
8180	4.37	27.75	0.07	2.17	2.31	0.17	2.72
8210	4.51	28.02	0.07	2.19	2.29	0.26	2.69
8270	4.43	27.60	0.06	2.16	2.27	0.48	2.70
8330	5.03	17.45	0.01	0.36	1.79	1.07	3.71
8390	4.81	17.08	0.01	0.36	1.77	1.15	3.55
8450	4.80	16.95	0.01	0.44	1.71	1.07	3.62
8510	5.16	16.84	0.01	0.40	1.87	0.96	3.95
8570	5.22	16.71	0.01	0.36	1.93	0.98	4.00

Wt% of Major Elements							
Sample	Al	Si	P	S	K	Ca	Fe
8630	5.10	16.24	0.01	0.35	1.89	0.89	3.94
8690	4.78	15.41	0.01	0.38	1.83	1.08	3.96
8750	4.82	16.03	0.01	0.51	1.88	1.20	4.00
8810	4.79	16.02	0.01	0.48	1.85	1.20	3.96
8870	3.40	18.42	0.01	0.34	1.30	0.95	3.85
8930	3.76	19.14	0.02	0.34	1.40	1.05	4.69
8990	3.58	19.83	0.02	0.38	1.35	1.02	3.72
9050	3.80	19.91	0.02	0.35	1.37	0.98	3.98
9110	4.19	19.89	0.02	0.36	1.52	0.74	4.49
9170	3.87	20.57	0.02	0.33	1.46	0.68	4.39
9230	3.50	17.71	0.01	0.33	1.41	0.67	4.10
9290	4.50	16.26	0.00	0.32	1.69	0.97	3.69
9350	4.67	16.94	0.01	0.35	1.74	0.81	3.76
9410	4.19	15.87	0.01	0.40	1.47	0.93	3.23
9470	4.53	17.31	0.01	0.35	1.55	0.59	3.36
9530	4.22	18.96	0.02	0.47	1.56	1.21	3.19
9590	5.11	16.59	0.01	0.31	1.81	0.64	3.82
9650	2.45	24.02	0.02	0.31	0.78	1.23	2.48
9710	4.08	19.21	0.02	0.59	1.57	1.35	3.10
9770	4.77	15.69	0.00	0.29	1.79	0.59	3.71
9830	4.06	19.31	0.02	0.71	1.53	1.61	2.94
9890	3.84	17.93	0.01	0.36	1.60	0.71	3.01
9950	4.24	19.75	0.01	0.38	1.56	0.84	3.05
10010	5.35	15.17	0.02	0.61	1.10	1.47	3.40
10070	5.56	16.01	0.03	0.74	1.20	1.43	3.17
10130	5.11	14.97	0.02	0.75	1.13	1.16	2.91
10190	5.02	14.70	0.02	0.73	1.12	1.31	3.04
10250	4.90	16.01	0.01	0.51	1.54	1.24	3.62
10310	4.96	17.07	0.01	0.35	1.80	1.04	3.72
10370	4.88	17.29	0.01	0.36	1.76	1.15	3.63
10430	4.72	16.70	0.01	0.40	1.73	1.08	3.55
10490	5.15	17.21	0.01	0.43	1.82	0.99	3.88
10550	5.17	16.64	0.01	0.36	1.91	0.97	3.95
10610	5.17	16.53	0.01	0.36	1.90	0.93	3.95
10670	4.97	15.78	0.01	0.36	1.90	1.01	4.02
10730	4.67	15.55	0.01	0.47	1.82	1.16	3.93
10790	4.86	16.09	0.01	0.49	1.87	1.19	4.00
10850	3.86	17.70	0.01	0.39	1.48	1.05	3.82
10910	3.63	18.80	0.01	0.34	1.37	1.00	4.52
10970	3.62	19.54	0.02	0.39	1.35	1.06	3.97
11030	3.72	19.90	0.02	0.33	1.37	0.98	3.94
11090	4.06	20.02	0.02	0.37	1.47	0.82	4.15
11150	3.94	20.34	0.02	0.34	1.44	0.71	4.72

Precision of major element analysis on standard using HHXRF												
	Mg	Al	Si	P	S	K	Ca	Ti	V (ppm)	Cr (ppm)	Mn	Fe
RTC-W-220 (1)	0.58	4.55	28.37	0.07	2.29	2.31	0.15	0.27	914.62	100.62	0.02	2.68
RTC-W-220 (2)	0.54	4.50	28.37	0.07	2.22	2.33	0.20	0.27	929.38	105.19	0.02	2.71
RTC-W-220 (3)	0.41	4.32	27.58	0.07	2.17	2.30	0.15	0.27	912.09	106.23	0.02	2.73
RTC-W-220 (4)	0.41	4.48	27.94	0.07	2.22	2.28	0.13	0.26	895.14	102.11	0.02	2.71
RTC-W-220 (5)	0.46	4.57	28.14	0.07	2.18	2.30	0.23	0.27	919.89	106.69	0.02	2.68
RTC-W-220 (6)	0.42	4.49	27.97	0.08	2.17	2.28	0.41	0.26	905.63	106.06	0.02	2.67
RTC-W-220 (7)	0.50	4.50	27.94	0.07	2.18	2.27	0.49	0.27	898.62	102.67	0.02	2.68
RTC-W-220 (8)	0.51	4.41	27.40	0.06	2.15	2.26	0.48	0.26	877.67	102.97	0.02	2.74
RTC-W-220 (9)	0.47	4.39	27.47	0.07	2.16	2.27	0.48	0.26	885.54	100.55	0.02	2.68
RTC-W-220 (10)	0.33	4.23	26.44	0.07	2.06	2.21	0.51	0.26	879.49	102.92	0.02	2.70
RTC-W-220 (11)	0.46	4.40	28.01	0.07	2.21	2.32	0.13	0.28	936.65	102.36	0.02	2.74
RTC-W-220 (12)	0.44	4.33	28.00	0.07	2.19	2.31	0.13	0.27	917.15	107.90	0.02	2.77
RTC-W-220 (13)	0.52	4.43	28.00	0.06	2.20	2.29	0.12	0.26	886.38	101.28	0.02	2.71
RTC-W-220 (14)	0.48	4.44	27.95	0.06	2.19	2.28	0.10	0.26	912.32	98.63	0.02	2.65
RTC-W-220 (15)	0.43	4.35	27.88	0.07	2.18	2.31	0.12	0.26	908.43	104.64	0.02	2.72
RTC-W-220 (16)	0.44	4.45	28.03	0.07	2.16	2.31	0.11	0.27	919.36	104.60	0.02	2.73
RTC-W-220 (17)	0.29	4.03	26.17	0.06	2.08	2.25	0.15	0.26	889.72	105.96	0.02	2.71
RTC-W-220 (18)	0.35	4.26	27.28	0.07	2.16	2.29	0.15	0.26	918.21	99.65	0.02	2.70
RTC-W-220 (19)	0.34	4.32	27.32	0.07	2.17	2.27	0.14	0.26	904.81	107.31	0.02	2.67
RTC-W-220 (20)	0.37	4.28	27.29	0.07	2.11	2.29	0.16	0.27	896.72	106.15	0.02	2.71
Average	0.44	4.39	27.68	0.07	2.17	2.29	0.23	0.26	905.39	103.72	0.02	2.70
Standard Deviation	0.08	0.13	0.58	0.00	0.05	0.03	0.15	0.00	16.41	2.72	0.00	0.03
Reported Values	0.67	4.96	32.60	0.07	3.34	2.07	0.13	0.23	928.00	110.00	0.02	2.93
Precision of major element analysis on standard using HHXRF												
	Mg	Al	Si	P	S	K	Ca	Ti	V (ppm)	Cr (ppm)	Mn	Fe
Bruker Duplex 2205 (1)	3.74	1.33	1.81	0.12	1.54	0.11	0.19	0.13	1373.44	-1631.92	13.45	22.35
Bruker Duplex 2205 (2)	2.96	1.28	1.76	0.10	1.38	0.15	0.22	0.13	1343.30	-281.43	12.88	21.99
Bruker Duplex 2205 (3)	2.81	1.24	1.75	0.10	1.39	0.11	0.20	0.13	1339.18	-636.01	13.03	21.99
Bruker Duplex 2205 (4)	3.12	1.15	1.77	0.10	1.40	0.01	0.19	0.12	1318.25	-681.24	13.05	22.13
Bruker Duplex 2205 (5)	2.73	1.23	1.98	0.09	1.38	0.27	0.26	0.12	1320.96	664.52	12.47	21.68
Bruker Duplex 2205 (6)	2.65	1.24	2.00	0.10	1.39	0.06	0.37	0.12	1289.32	220.81	12.67	21.92
Bruker Duplex 2205 (7)	2.88	1.27	1.97	0.10	1.42	0.07	0.46	0.13	1315.66	-125.28	12.81	21.79
Bruker Duplex 2205 (8)	2.81	1.25	1.95	0.10	1.39	0.08	0.45	0.12	1304.36	318.95	12.62	21.91
Bruker Duplex 2205 (9)	2.55	1.17	1.90	0.09	1.30	0.05	0.42	0.12	1256.10	1841.62	11.96	21.39
Bruker Duplex 2205 (10)	2.91	1.26	1.97	0.10	1.40	0.04	0.46	0.12	1276.55	366.60	12.60	21.77
Bruker Duplex 2205 (11)	2.31	1.05	1.71	0.08	1.28	0.07	0.17	0.12	1274.88	1600.96	12.07	21.40
Bruker Duplex 2205 (12)	2.54	1.13	1.73	0.09	1.32	0.09	0.17	0.13	1287.78	871.11	12.38	21.52
Bruker Duplex 2205 (13)	2.80	1.19	1.76	0.11	1.39	0.05	0.18	0.13	1319.30	-658.02	13.04	21.93
Bruker Duplex 2205 (14)	2.78	1.18	1.69	0.10	1.35	0.11	0.18	0.12	1314.87	467.57	12.56	21.93
Bruker Duplex 2205 (15)	3.03	1.17	1.69	0.09	1.36	0.04	0.17	0.12	1292.40	-215.31	12.86	21.97
Bruker Duplex 2205 (16)	2.84	1.23	1.70	0.09	1.29	0.21	0.17	0.12	1316.76	1328.76	12.18	21.48
Bruker Duplex 2205 (17)	2.84	1.17	1.71	0.09	1.35	0.23	0.19	0.12	1325.96	518.10	12.54	21.69
Bruker Duplex 2205 (18)	2.73	1.25	1.87	0.09	1.34	0.04	0.17	0.12	1300.57	20.71	12.75	21.87
Bruker Duplex 2205 (19)	2.90	1.18	2.01	0.09	1.35	0.19	0.20	0.12	1328.51	183.36	12.68	21.62
Bruker Duplex 2205 (20)	2.80	1.22	1.95	0.09	1.36	0.24	0.20	0.13	1299.73	411.53	12.59	21.70
Average	2.84	1.21	1.83	0.10	1.37	0.11	0.25	0.12	1309.89	229.27	12.66	21.80
Standard Deviation	0.28	0.06	0.12	0.01	0.06	0.08	0.11	0.00	26.83	825.60	0.36	0.25

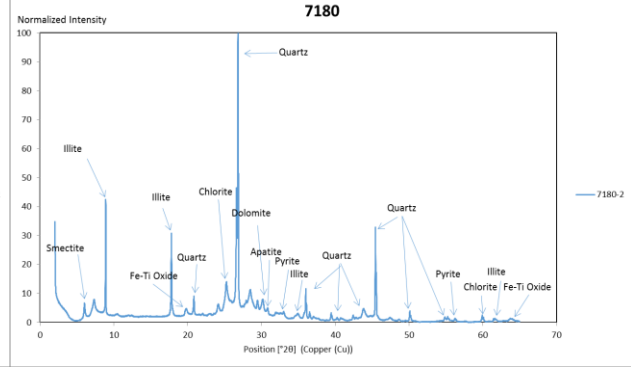
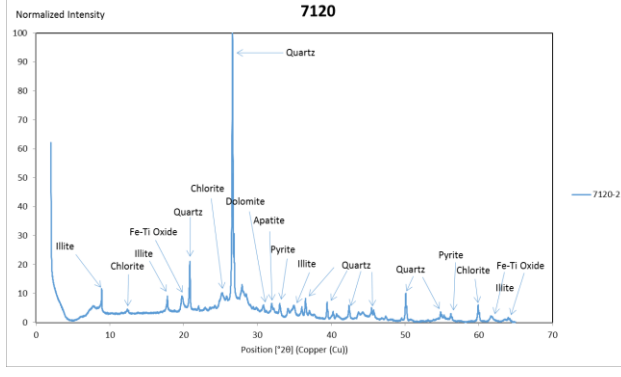
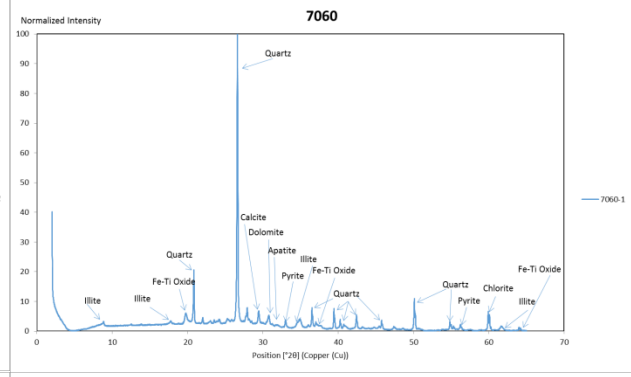
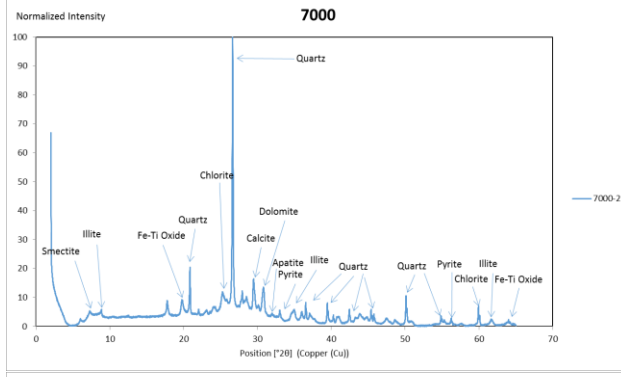
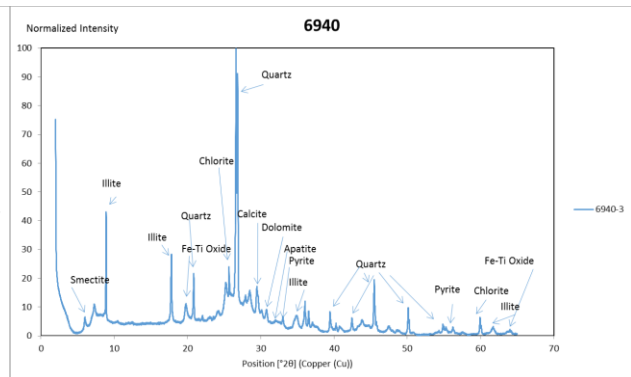
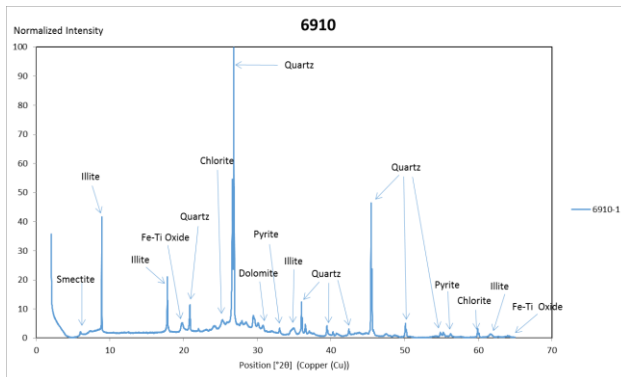
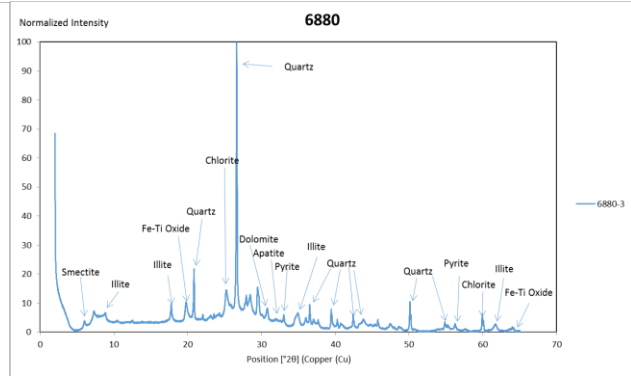
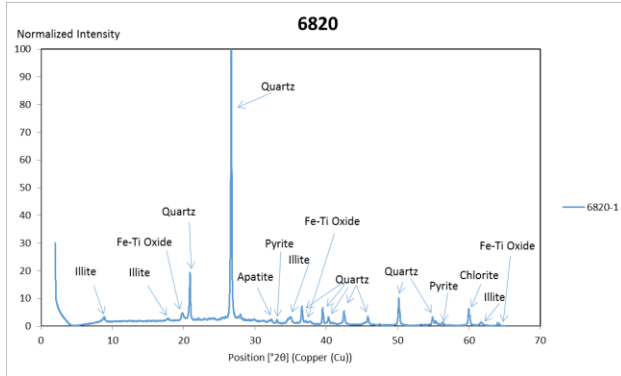
Appendix C.1 - 1 precision of major element analysis on standard using HHXRF using RTC-W220 (Rowe et al., 2010) and Bruker Duplex 2205.

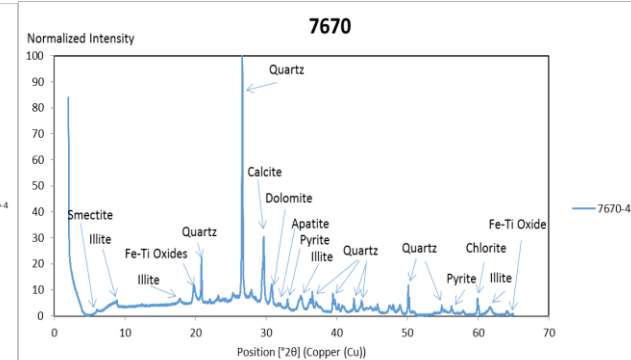
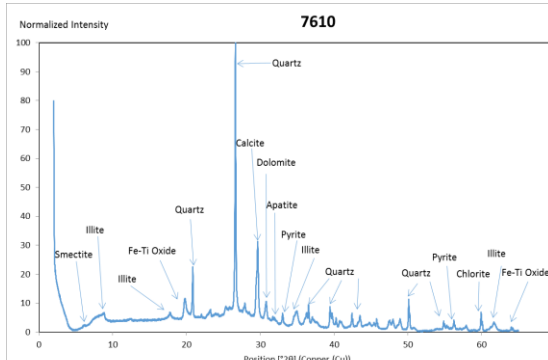
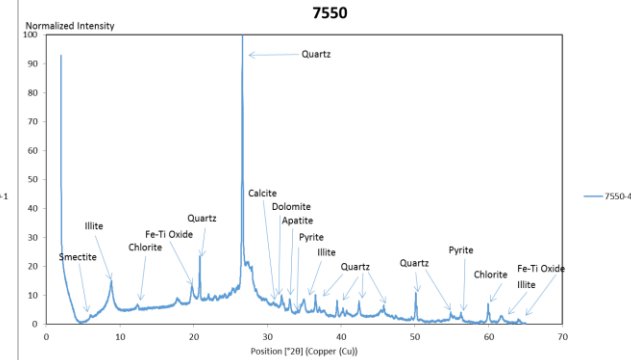
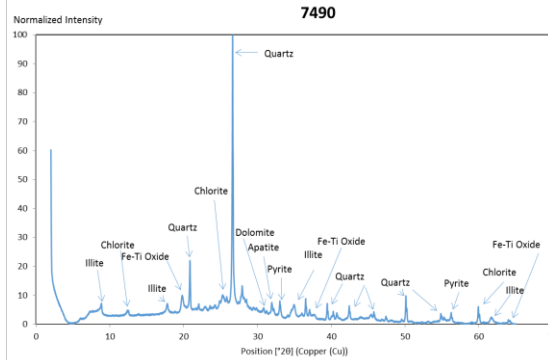
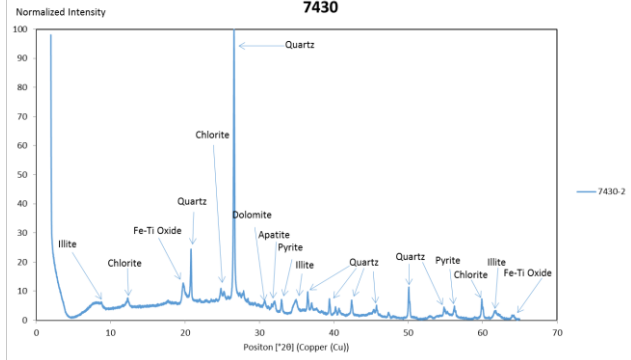
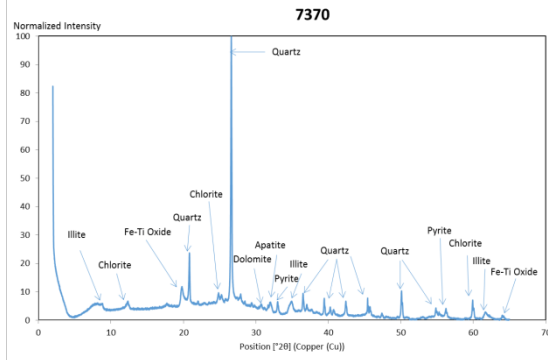
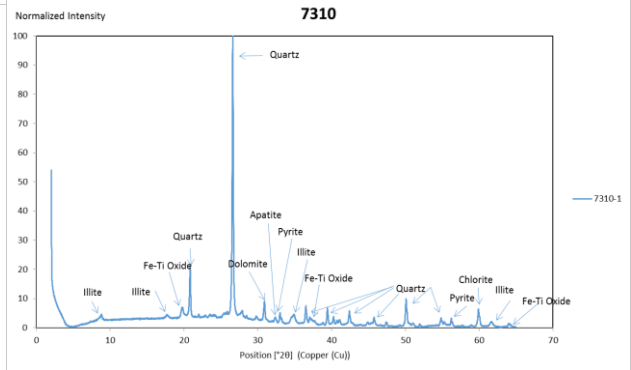
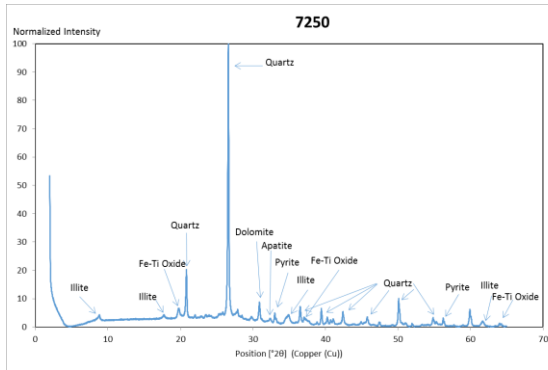
Precision of trace element analysis of standard using HHXRF																
	Ba	Co	Ni	Cu	Zn	Ga	As	Pb	Th	Rb	U	Sr	Y	Zr	Nb	Mo
RTC-W-220 (1)	0.2001	0.0017	0.0144	0.0130	0.0856	0.0018	0.0025	0.0019	0.0011	0.0135	0.0010	0.0052	0.0034	0.0114	0.0013	0.0070
RTC-W-220 (2)	0.0996	0.0017	0.0144	0.0133	0.0815	0.0016	0.0027	0.0019	0.0011	0.0137	0.0013	0.0053	0.0033	0.0114	0.0012	0.0074
RTC-W-220 (3)	0.2561	0.0014	0.0145	0.0130	0.0866	0.0017	0.0022	0.0018	0.0011	0.0136	0.0013	0.0059	0.0034	0.0113	0.0013	0.0073
RTC-W-220 (4)	0.2251	0.0017	0.0143	0.0130	0.0808	0.0016	0.0023	0.0018	0.0011	0.0133	0.0015	0.0054	0.0033	0.0114	0.0012	0.0072
RTC-W-220 (5)	0.2154	0.0016	0.0147	0.0129	0.0800	0.0018	0.0022	0.0018	0.0011	0.0134	0.0017	0.0054	0.0032	0.0113	0.0012	0.0071
RTC-W-220 (6)	0.1434	0.0017	0.0142	0.0130	0.0794	0.0018	0.0020	0.0017	0.0011	0.0143	0.0011	0.0056	0.0034	0.0113	0.0012	0.0073
RTC-W-220 (7)	0.0820	0.0015	0.0146	0.0131	0.0863	0.0017	0.0020	0.0017	0.0011	0.0131	0.0015	0.0061	0.0034	0.0114	0.0012	0.0072
RTC-W-220 (8)	0.2738	0.0014	0.0149	0.0129	0.0853	0.0018	0.0025	0.0019	0.0011	0.0136	0.0018	0.0060	0.0032	0.0115	0.0013	0.0076
RTC-W-220 (9)	0.1357	0.0015	0.0146	0.0128	0.0860	0.0016	0.0022	0.0017	0.0011	0.0134	0.0017	0.0057	0.0032	0.0113	0.0013	0.0071
RTC-W-220 (10)	0.2330	0.0016	0.0147	0.0131	0.0835	0.0017	0.0021	0.0017	0.0011	0.0137	0.0013	0.0058	0.0034	0.0114	0.0013	0.0074
RTC-W-220 (11)	0.2893	0.0016	0.0144	0.0149	0.0835	0.0018	0.0023	0.0019	0.0011	0.0136	0.0013	0.0056	0.0032	0.0116	0.0012	0.0071
RTC-W-220 (12)	0.1771	0.0014	0.0141	0.0132	0.0789	0.0017	0.0024	0.0019	0.0011	0.0135	0.0014	0.0053	0.0033	0.0114	0.0012	0.0070
RTC-W-220 (13)	0.1876	0.0015	0.0134	0.0128	0.0805	0.0018	0.0020	0.0017	0.0011	0.0133	0.0019	0.0057	0.0032	0.0117	0.0013	0.0072
RTC-W-220 (14)	0.2108	0.0015	0.0144	0.0130	0.0792	0.0019	0.0020	0.0018	0.0011	0.0137	0.0012	0.0050	0.0032	0.0116	0.0012	0.0069
RTC-W-220 (15)	0.1802	0.0017	0.0147	0.0130	0.0802	0.0017	0.0021	0.0017	0.0011	0.0132	0.0022	0.0062	0.0031	0.0114	0.0012	0.0076
RTC-W-220 (16)	0.1230	0.0018	0.0144	0.0139	0.0812	0.0017	0.0019	0.0017	0.0011	0.0138	0.0016	0.0064	0.0034	0.0114	0.0012	0.0078
RTC-W-220 (17)	0.2460	0.0016	0.0139	0.0130	0.0797	0.0017	0.0021	0.0017	0.0011	0.0134	0.0018	0.0055	0.0032	0.0113	0.0012	0.0072
RTC-W-220 (18)	0.1701	0.0018	0.0148	0.0132	0.0809	0.0017	0.0024	0.0018	0.0011	0.0132	0.0015	0.0054	0.0033	0.0115	0.0012	0.0070
Average	0.1916	0.0016	0.0144	0.0132	0.0822	0.0017	0.0022	0.0018	0.0011	0.0135	0.0015	0.0056	0.0033	0.0114	0.0012	0.0072
Standard Deviation	0.0588	0.0001	0.0004	0.0005	0.0027	0.0001	0.0002	0.0001	0.0000	0.0003	0.0003	0.0004	0.0001	0.0001	0.0000	0.0002
Reported Values	0.2090	N/A	0.0130	0.0083	0.0823	N/A	N/A	N/A	0.0008	0.1220	0.0018	0.0076	0.0035	0.0080	0.0001	0.0079
Precision of trace element analysis of standard using HHXRF																
	Ba	Co	Ni	Cu	Zn	Ga	As	Pb	Th	Rb	U	Sr	Y	Zr	Nb	Mo
Bruker Duplex 2205 (1)	0.2352	1.0744	-25.9125	3.7960	0.0053	0.0075	-0.0015	0.0021	0.0002	-0.0034	-0.0202	-0.0600	-0.0005	0.0097	0.0001	-0.9179
Bruker Duplex 2205 (2)	0.1057	1.0577	-25.6609	3.6506	0.0062	0.0070	0.0000	0.0027	0.0002	-0.0041	-0.0187	-0.0583	-0.0008	0.0094	0.0001	-0.8505
Bruker Duplex 2205 (3)	0.4296	1.0435	-24.9838	3.5860	0.0057	0.0074	-0.0017	0.0021	0.0002	-0.0019	-0.0223	-0.0609	-0.0004	0.0096	0.0002	-0.9354
Bruker Duplex 2205 (4)	-0.3819	1.0614	-25.4047	3.6921	0.0062	0.0069	-0.0003	0.0023	0.0002	-0.0022	-0.0201	-0.0574	-0.0005	0.0097	0.0001	-0.7877
Bruker Duplex 2205 (5)	-0.2437	1.0834	-25.9314	3.7656	0.0059	0.0073	-0.0011	0.0022	0.0002	-0.0024	-0.0204	-0.0591	-0.0006	0.0093	0.0002	-0.8654
Bruker Duplex 2205 (6)	-0.4674	1.0981	-26.4250	3.8220	0.0058	0.0076	-0.0012	0.0024	0.0002	-0.0027	-0.0208	-0.0603	-0.0003	0.0097	0.0000	-0.9134
Bruker Duplex 2205 (7)	-0.0968	1.0736	-25.7161	3.6915	0.0054	0.0077	-0.0004	0.0038	0.0002	-0.0030	-0.0194	-0.0574	-0.0002	0.0095	0.0002	-0.7779
Bruker Duplex 2205 (8)	-0.1120	1.0617	-25.5402	3.7575	0.0054	0.0078	-0.0022	0.0020	0.0002	-0.0020	-0.0209	-0.0591	-0.0005	0.0092	-0.0001	-0.8492
Bruker Duplex 2205 (9)	0.6072	1.0642	-25.5153	3.7796	0.0051	0.0078	-0.0016	0.0028	0.0001	-0.0023	-0.0224	-0.0618	-0.0003	0.0097	0.0001	-1.0005
Bruker Duplex 2205 (10)	0.6836	1.0649	-25.6430	3.6801	0.0056	0.0074	-0.0031	0.0012	0.0002	-0.0021	-0.0199	-0.0569	-0.0003	0.0093	0.0002	-0.7705
Bruker Duplex 2205 (11)	0.0984	1.0276	-24.7383	3.7966	0.0065	0.0076	0.0010	0.0038	0.0002	-0.0030	-0.0191	-0.0570	-0.0006	0.0093	0.0002	-0.7489
Bruker Duplex 2205 (12)	0.8375	1.0562	-25.4758	3.8396	0.0058	0.0076	-0.0007	0.0030	0.0001	-0.0029	-0.0216	-0.0598	-0.0004	0.0093	0.0002	-0.9196
Bruker Duplex 2205 (13)	0.1013	1.0541	-25.4454	3.8400	0.0061	0.0073	-0.0004	0.0029	0.0002	-0.0018	-0.0205	-0.0571	0.0003	0.0093	0.0001	-0.7369
Bruker Duplex 2205 (14)	-0.6270	1.0794	-25.9939	3.8740	0.0064	0.0075	0.0005	0.0034	0.0002	-0.0019	-0.0193	-0.0560	-0.0006	0.0090	-0.0001	-0.7259
Bruker Duplex 2205 (15)	0.1436	1.0661	-25.6923	3.8199	0.0058	0.0075	-0.0013	0.0026	0.0002	-0.0019	-0.0203	-0.0584	-0.0002	0.0094	0.0000	-0.8214
Bruker Duplex 2205 (16)	0.0031	1.0670	-25.7838	3.9578	0.0062	0.0083	-0.0034	0.0020	0.0002	-0.0024	-0.0203	-0.0579	-0.0002	0.0092	0.0001	-0.7884
Bruker Duplex 2205 (17)	-0.0997	1.0919	-25.9968	3.9327	0.0057	0.0080	0.0005	0.0040	0.0001	-0.0025	-0.0217	-0.0601	-0.0002	0.0096	0.0000	-0.9209
Bruker Duplex 2205 (18)	0.0917	1.0793	-26.0218	3.9080	0.0058	0.0078	-0.0013	0.0028	0.0001	-0.0027	-0.0210	-0.0576	0.0003	0.0094	0.0000	-0.8046
Average	0.1369	1.0652	-25.6435	3.8499	0.0060	0.0077	-0.0009	0.0028	0.0002	-0.0024	-0.0204	-0.0579	-0.0002	0.0093	0.0001	-0.8041
Standard Deviation	0.4260	0.0185	0.4030	0.0831	0.0003	0.0003	0.0015	0.0009	0.0000	0.0005	0.0009	0.0014	0.0003	0.0002	0.0001	0.0727

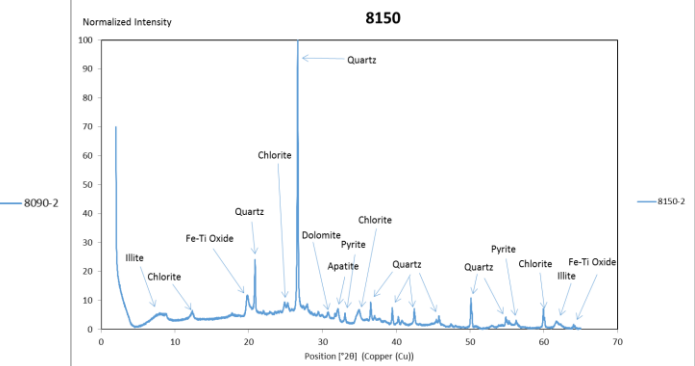
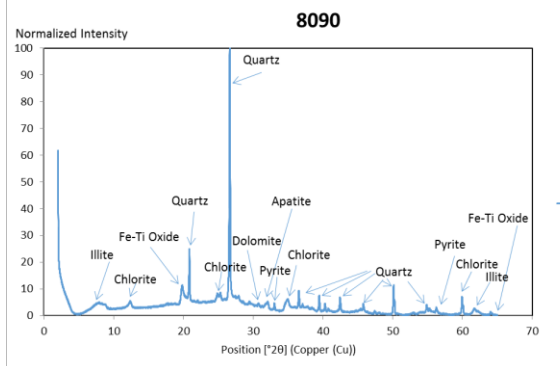
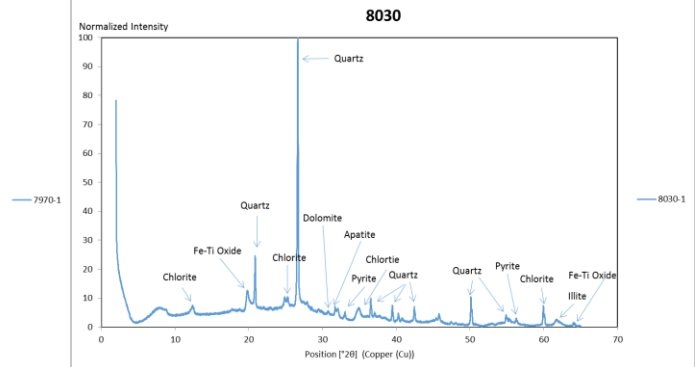
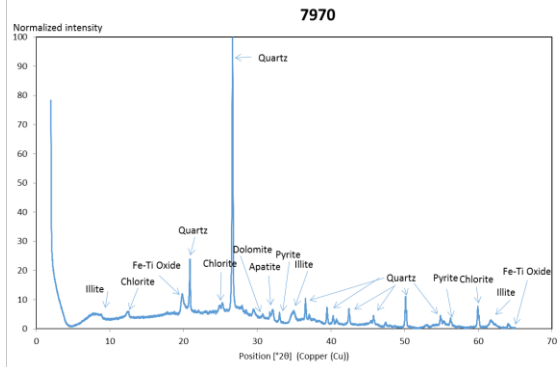
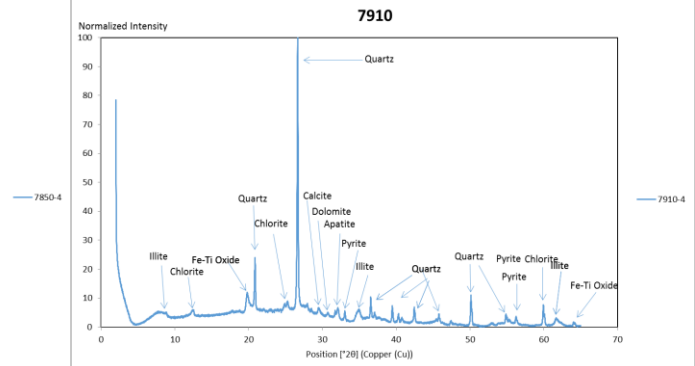
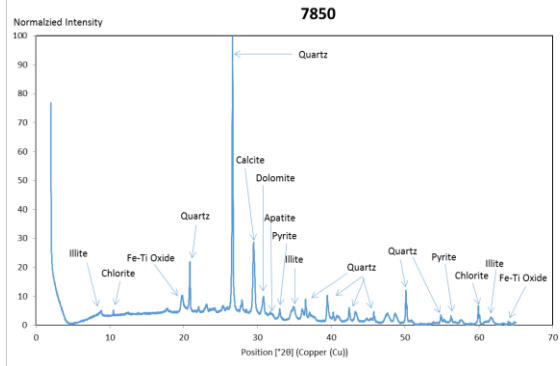
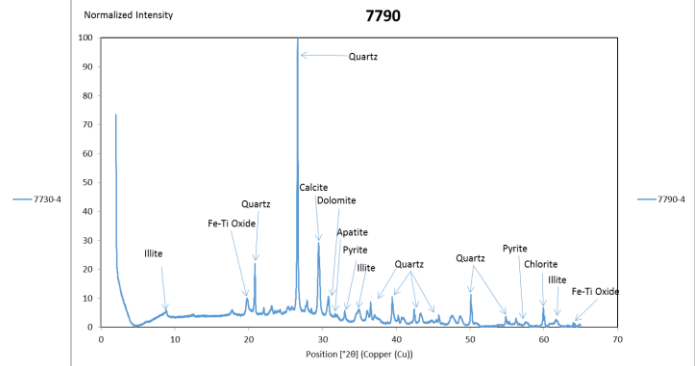
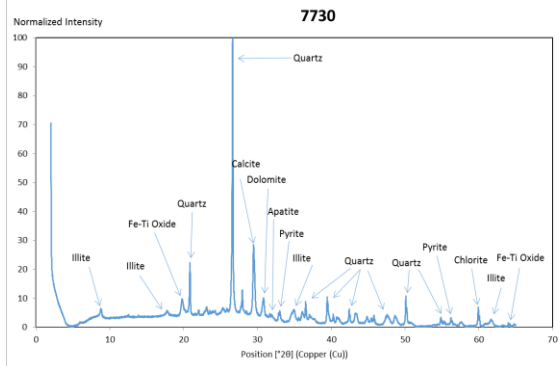
Appendix C.1 - 2 - Precision of trace element using HHXRF using RTC-W220 (Rowe et al., 2010) and Bruker Duplex 2205.

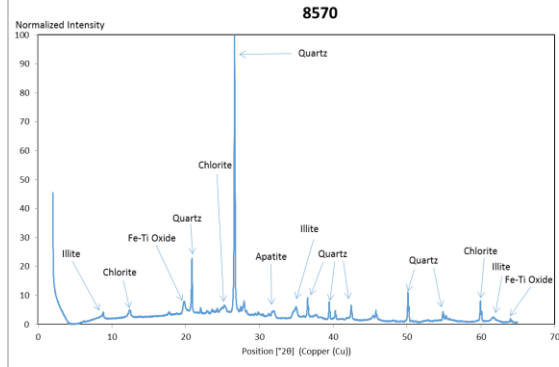
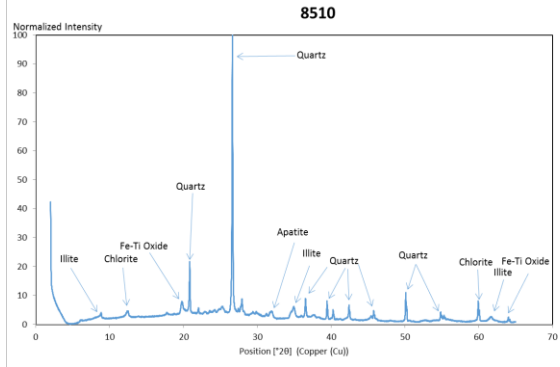
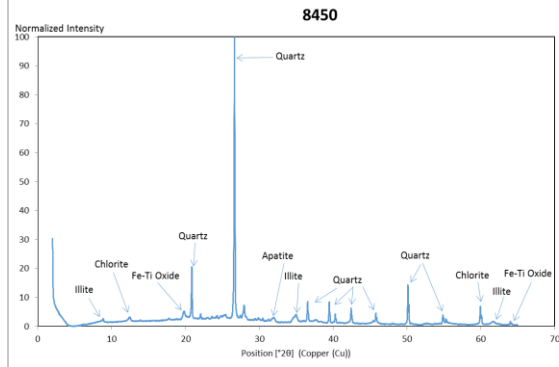
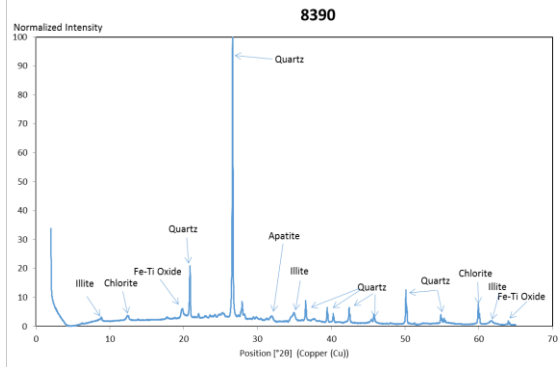
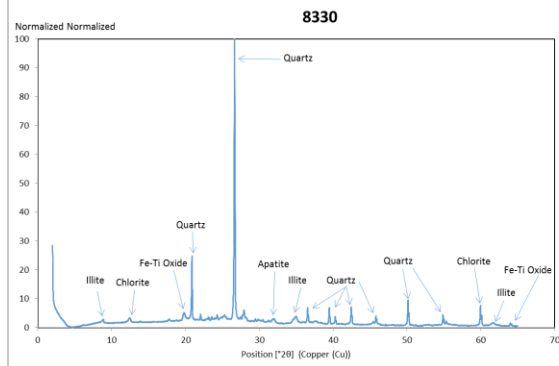
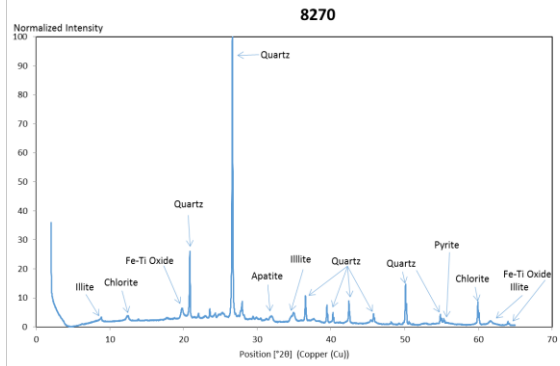
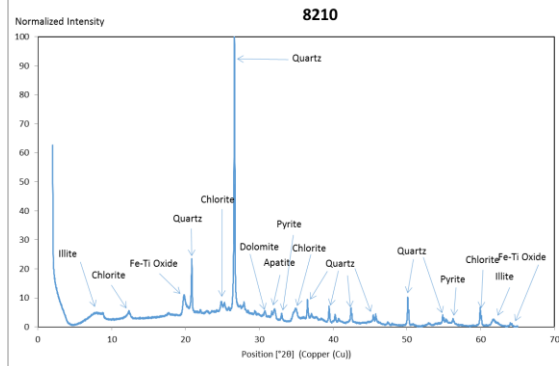
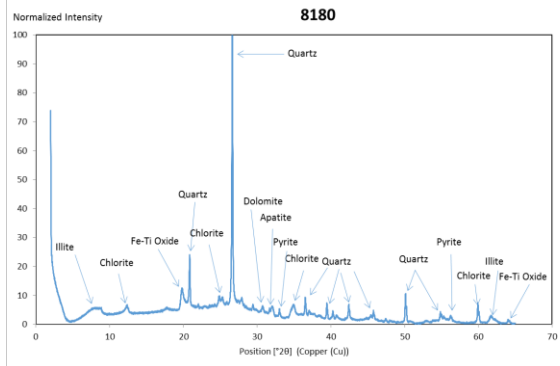
Appendix B - XRD Bulk Powder Data

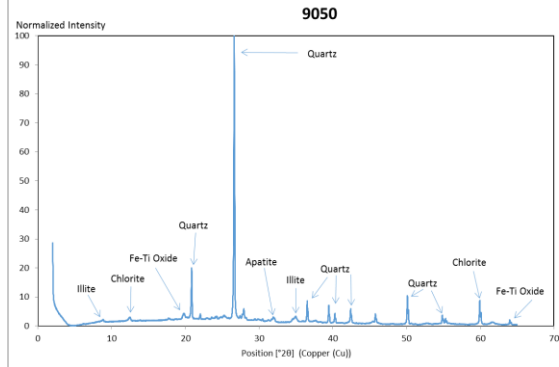
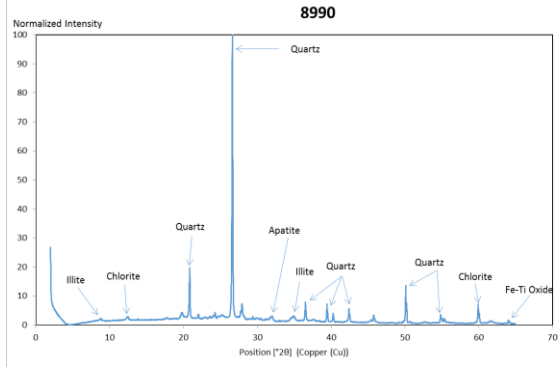
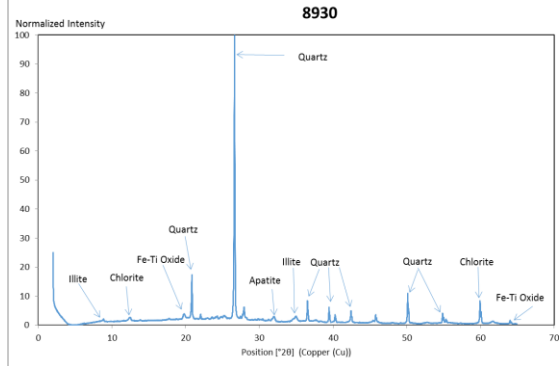
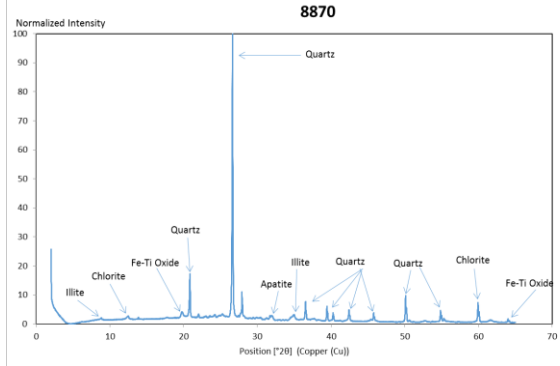
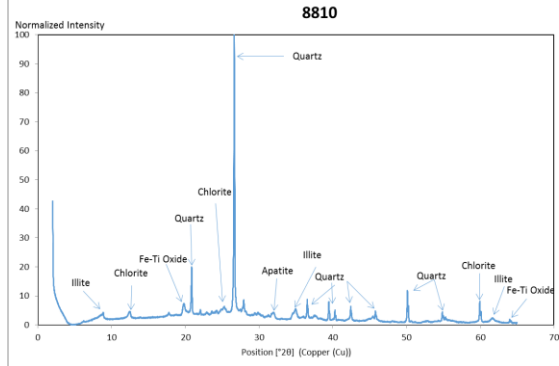
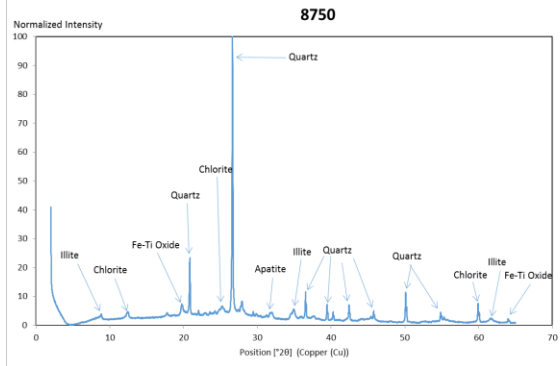
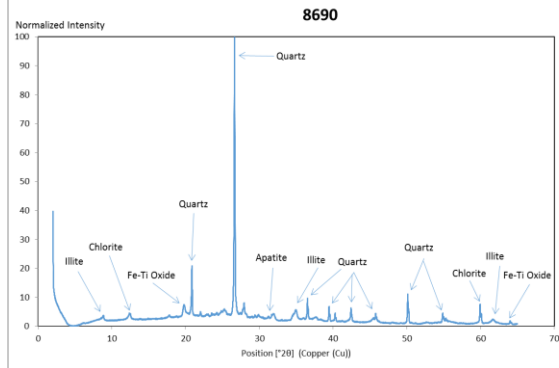
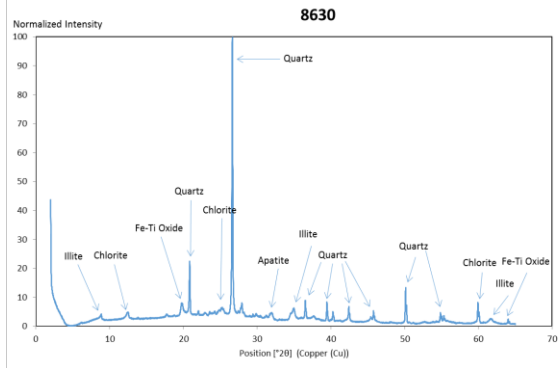
The XRD bulk powder data is presented here in Appendix B. This appendix contains diffractograms from some of the samples provided by Pablo Energy. The title of each diffractogram is given in measured distance this is because each sample is from the well path for each sample. Note that this includes diffractograms that were later determined to be of the Hunton Limestone and not of the Woodford Shale. The Hunton Limestone diffractograms were not focused on because of the study was focused on the Woodford Shale. The Hunton Limestone diffractograms were included to ensure completeness of the well path. The entire measured samples are from the start measured distance 6820 feet to the finish 11150 feet of the well path. Most of these samples are located within the Woodford Shale. The mineralogy of each sample is identified at each peak.

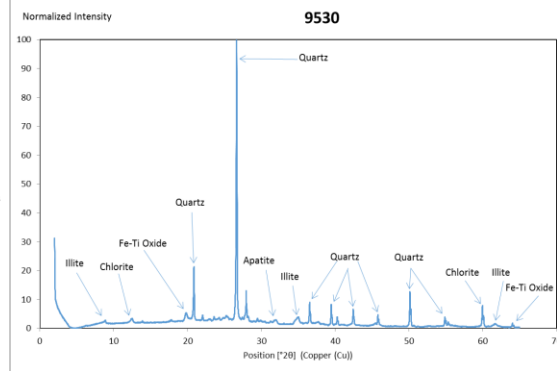
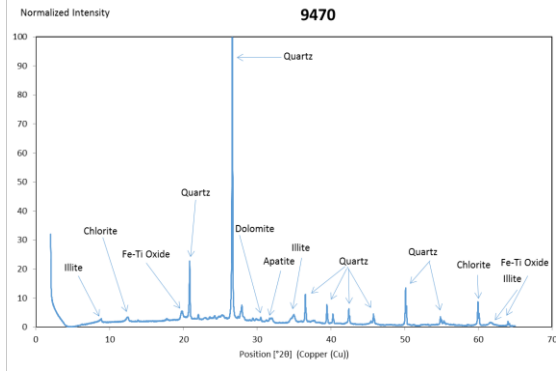
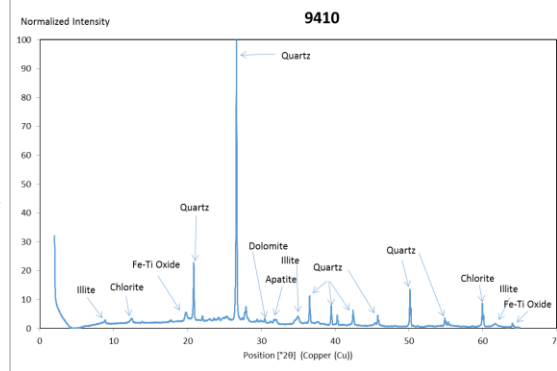
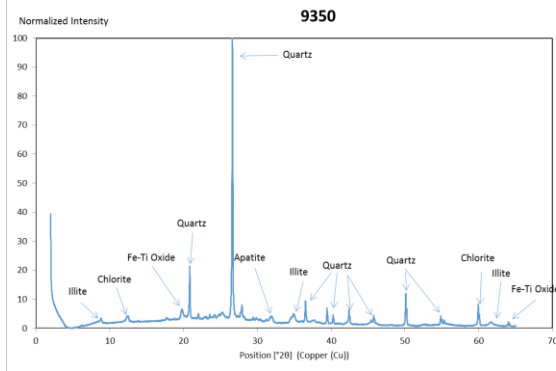
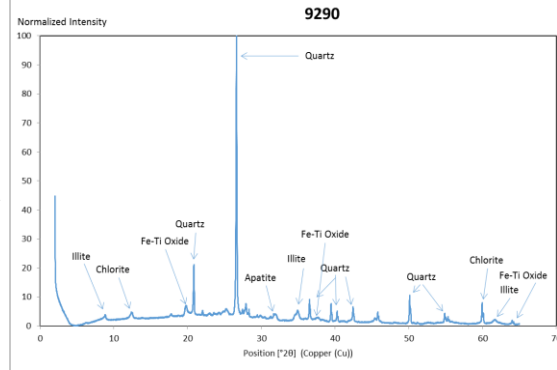
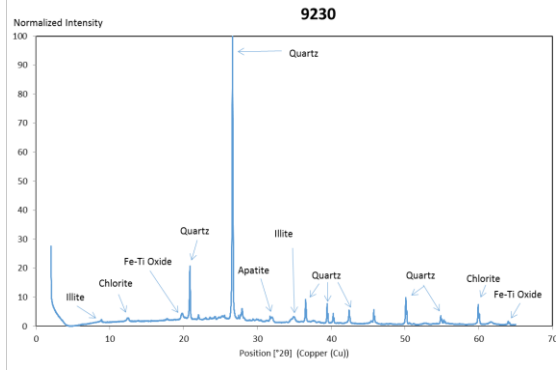
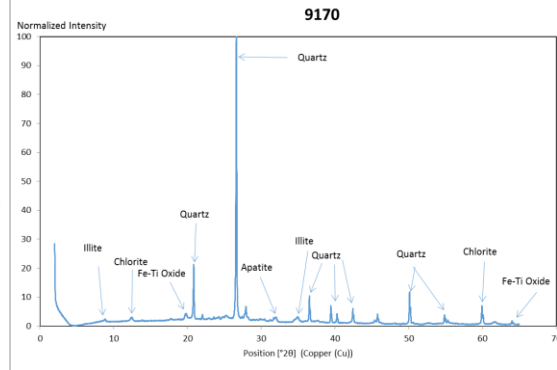
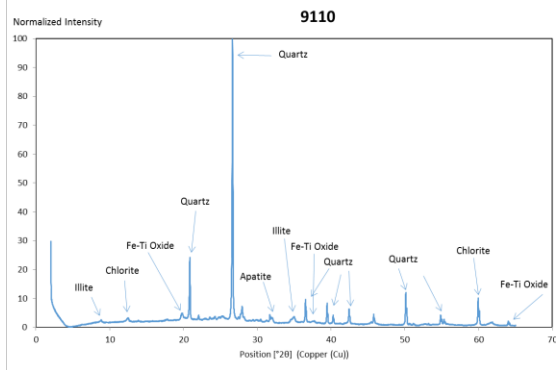


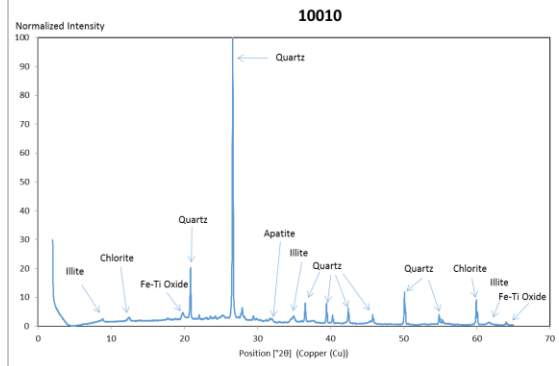
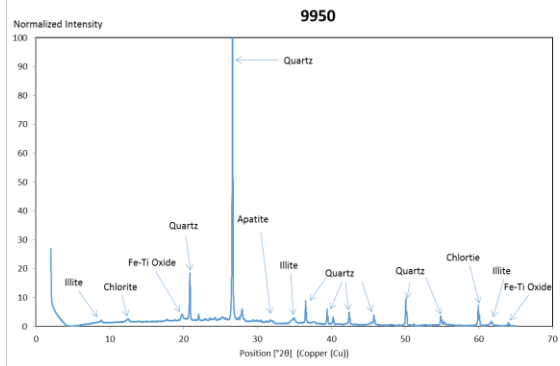
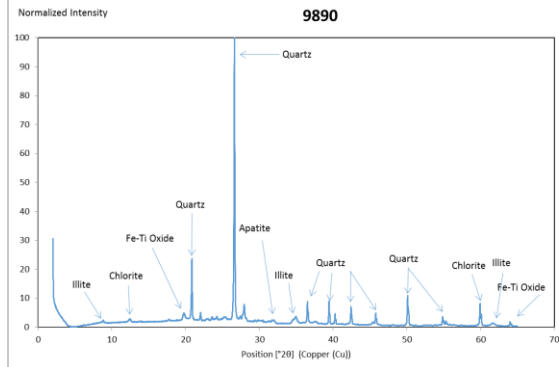
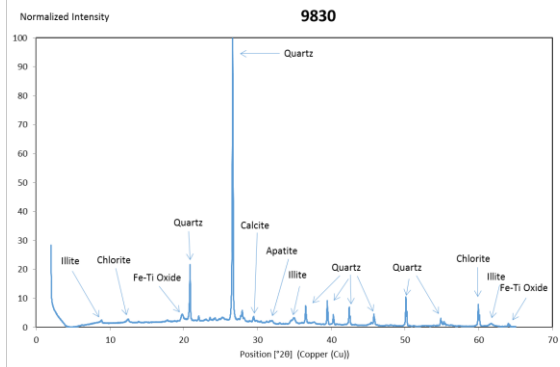
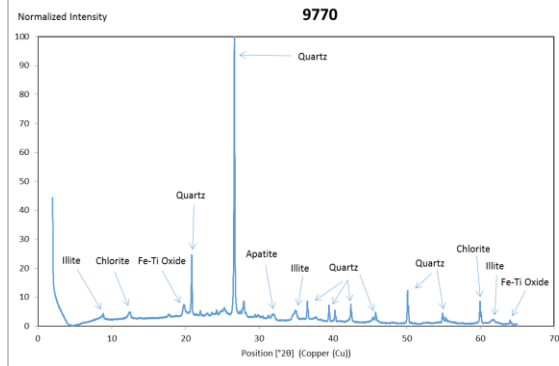
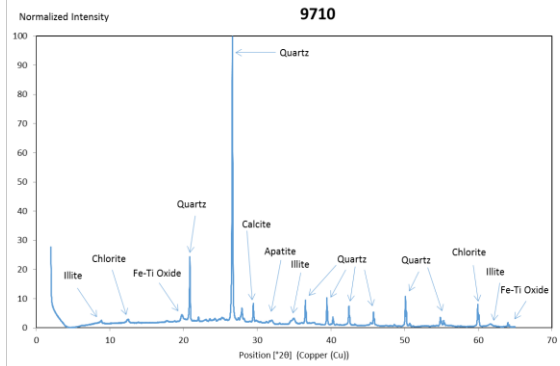
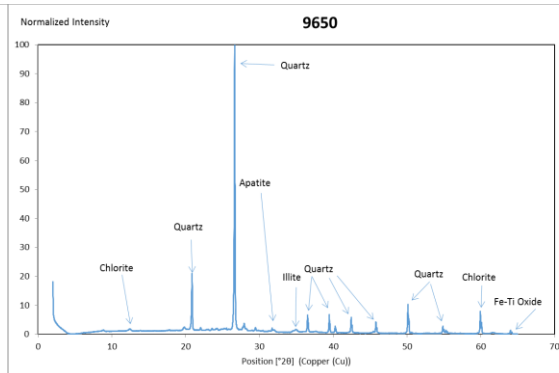
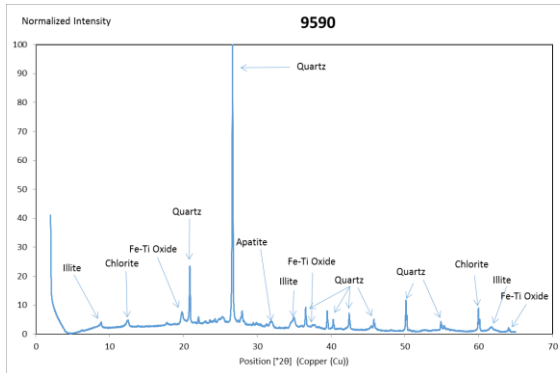


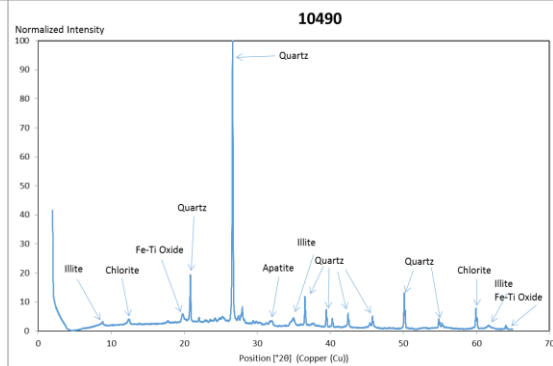
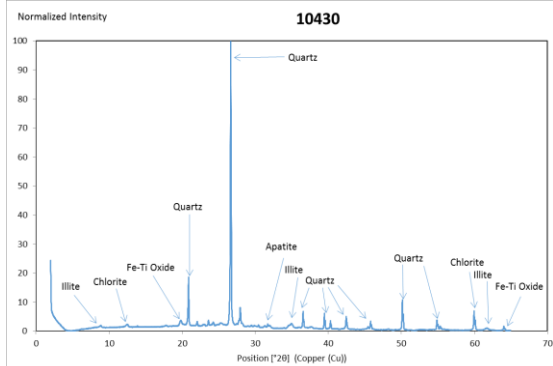
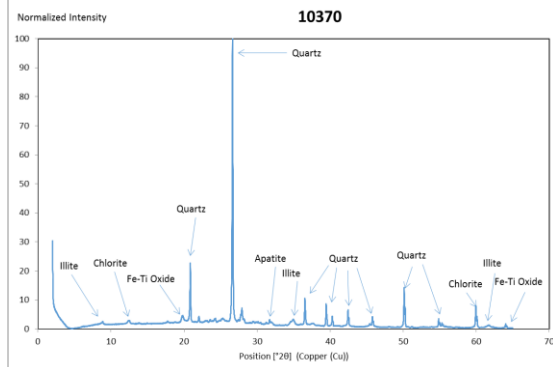
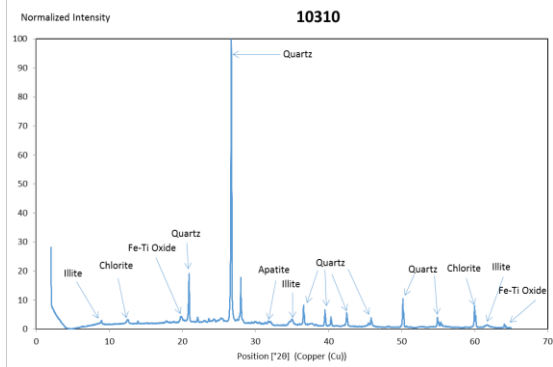
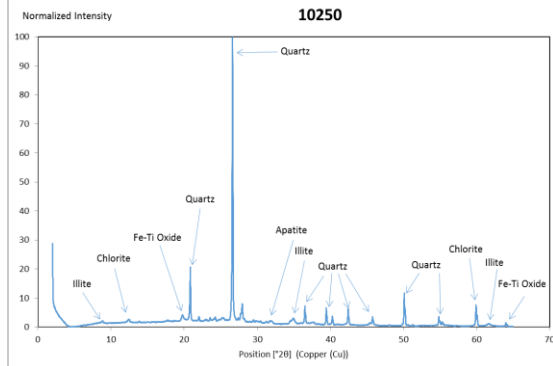
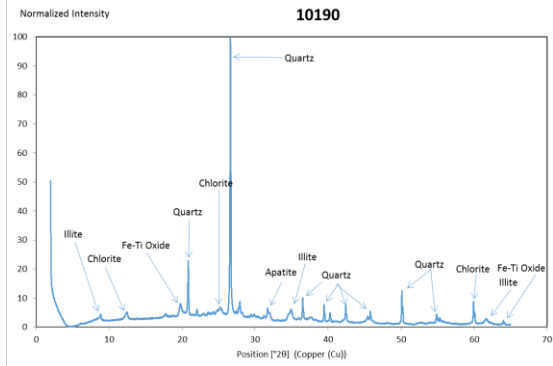
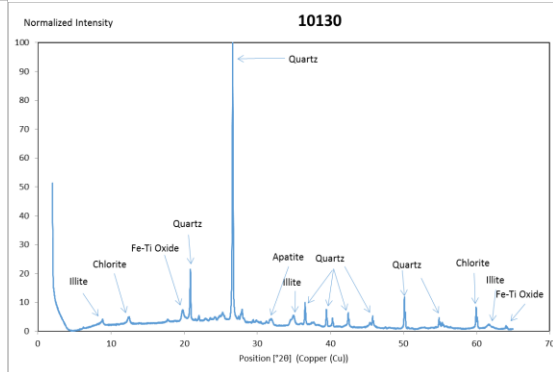
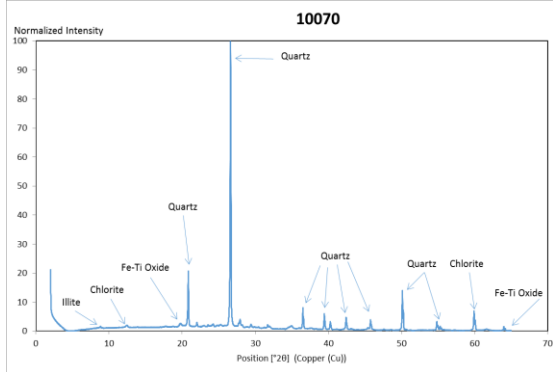


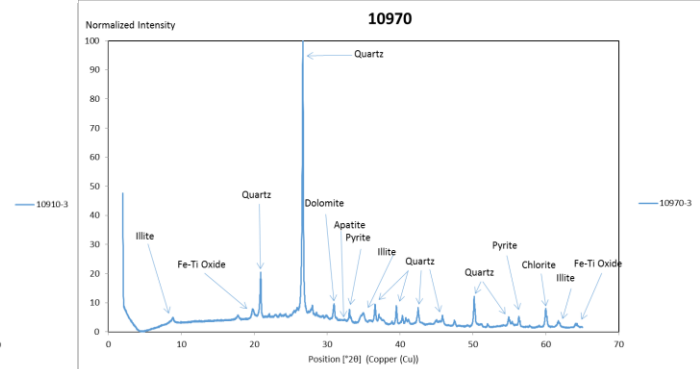
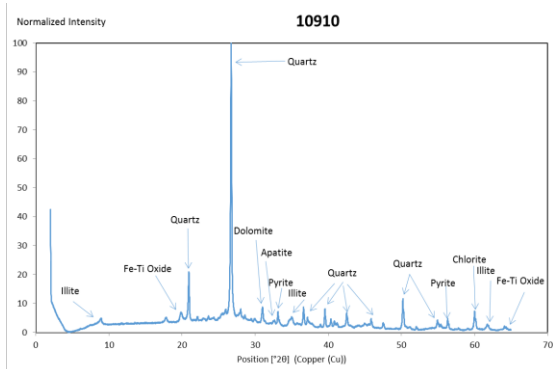
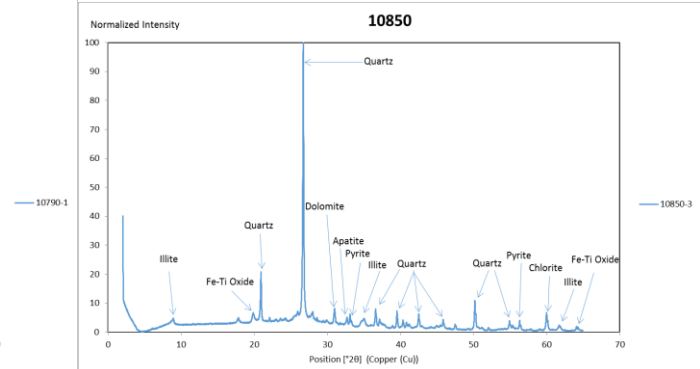
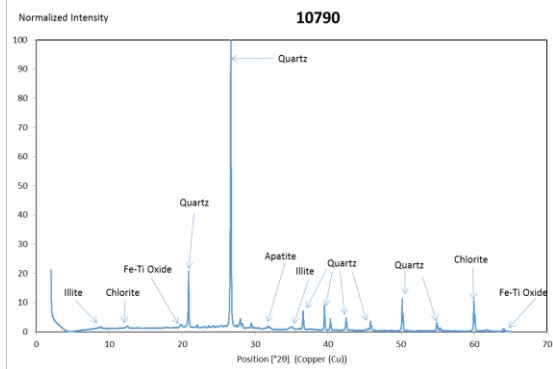
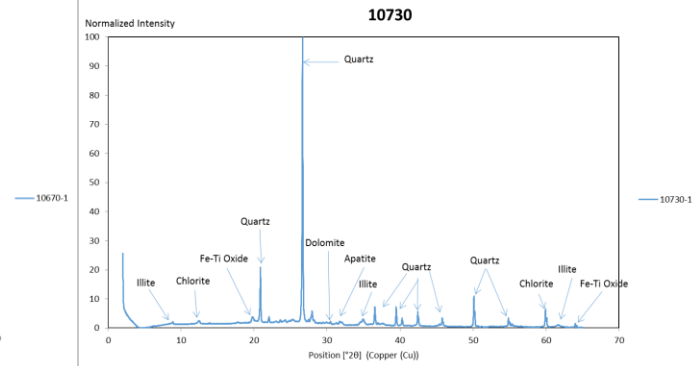
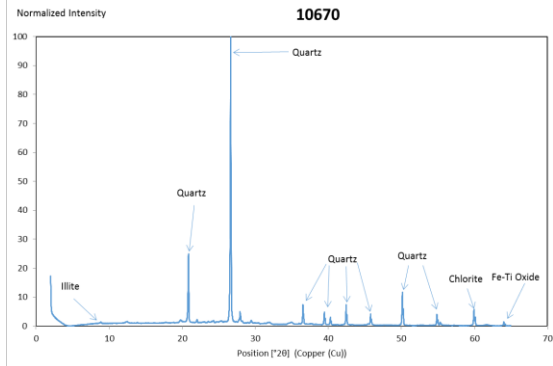
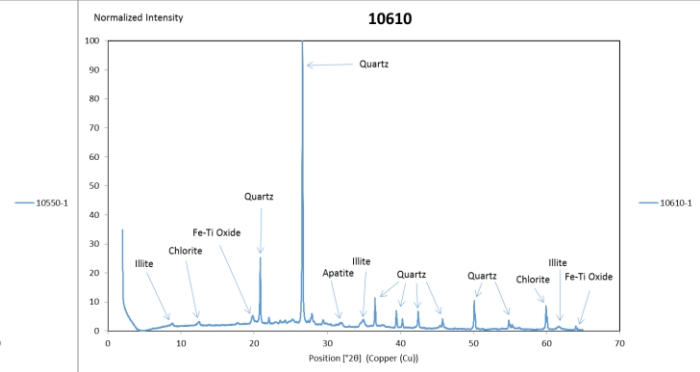
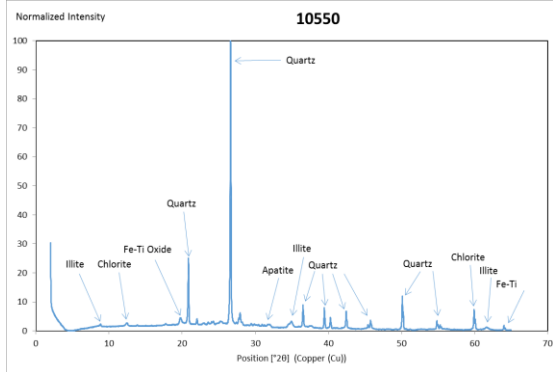


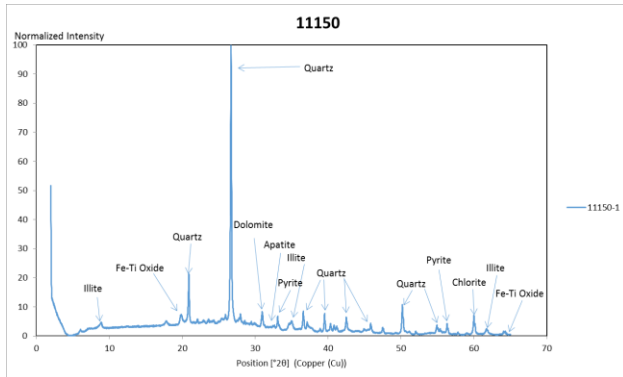
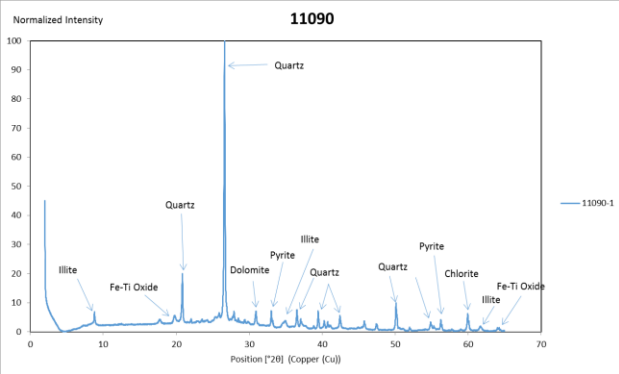
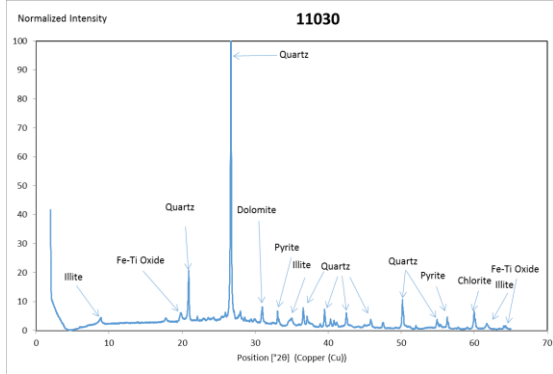












Appendix C - Loss on Ignition Data Tables

The Loss on Ignition data tables show the weight (grams) prior to entering the muffle furnace and weighed (grams) afterwards. The difference in weight (grams) is calculated to give the percentage LOI and then a proxy was used to calculate the TOC in wt%. The entire measured samples are from the start measured distance 6820 feet to the finish 11150 feet of the well path.

Sample	Weight Before (grams)	Weight After (grams)	Difference (grams)	LOI% (% loss)	Proxy TOC (Wt%)
6820	1.577	1.447	0.13	8.244	5.825
6880	3.226	2.892	0.334	11.549	8.601
6910	2.166	1.93	0.236	12.228	9.172
6940	2.706	2.403	0.303	12.609	9.492
7000	1.684	1.412	0.272	19.263	15.081
7060	2.591	2.334	0.257	11.011	8.149
7120	2.011	1.755	0.256	14.587	11.153
7180	2.726	2.374	0.352	14.827	11.355
7250	1.217	1.061	0.156	14.703	11.251
7310	1.712	1.5	0.212	14.133	10.772
7370	2.523	2.283	0.24	10.512	7.730
7430	0.987	0.804	0.183	22.761	18.019
7490	2.58	1.644	0.936	56.934	46.725
7550	2.449	1.915	0.534	27.885	22.323
7610	2.09	1.849	0.241	13.034	9.849
7670	1.829	1.62	0.209	12.901	9.737
7730	5.053	4.534	0.519	11.447	8.515
7790	2.999	2.639	0.36	13.642	10.359
7850	2.181	1.9	0.281	14.789	11.323
7910	1.484	1.306	0.178	13.629	10.349
7970	2.697	2.427	0.27	11.125	8.245
8030	6.408	5.754	0.654	11.366	8.447
8090	1.595	1.429	0.166	11.617	8.658
8150	4.464	3.972	0.492	12.387	9.305
8180	2.226	1.975	0.251	12.709	9.575
8210	3.454	3.097	0.357	11.527	8.583
8270	2.672	2.459	0.213	8.662	6.176
8330	3.981	3.646	0.335	9.188	6.618
8390	3.785	3.444	0.341	9.901	7.217
8450	1.498	1.349	0.149	11.045	8.178
8510	2.462	2.261	0.201	8.890	6.367
8570	2.486	2.271	0.215	9.467	6.852
8630	2.667	2.431	0.236	9.708	7.055
8690	2.748	2.443	0.305	12.485	9.387
8750	1.862	1.661	0.201	12.101	9.065
8810	1.78	1.635	0.145	8.869	6.350
8870	2.39	2.201	0.189	8.587	6.113
8930	1.478	1.363	0.115	8.437	5.987
8990	2.156	1.965	0.191	9.720	7.065

Sample	Weight Before (grams)	Weight After (grams)	Difference (grams)	LOI% (% loss)	Proxy TOC (Wt%)
9050	2.123	1.943	0.18	9.264	6.682
9110	2.441	2.245	0.196	8.731	6.234
9170	2.34	2.138	0.202	9.448	6.836
9230	1.436	1.31	0.126	9.618	6.979
9290	3.352	3.053	0.299	9.794	7.127
9350	1.955	1.771	0.184	10.390	7.627
9410	3.078	2.815	0.263	9.343	6.748
9470	3.533	3.215	0.318	9.891	7.209
9530	4.124	3.793	0.331	8.727	6.230
9590	4.538	4.149	0.389	9.376	6.776
9650	3.887	3.632	0.255	7.021	4.798
9710	4.076	3.768	0.308	8.174	5.766
9770	3.813	3.46	0.353	10.202	7.470
9830	3.237	2.983	0.254	8.515	6.053
9890	5.58	5.123	0.457	8.921	6.393
9950	5.001	4.55	0.451	9.912	7.226
10010	3.196	2.959	0.237	8.009	5.628
10070	5.265	4.966	0.299	6.021	3.958
10130	2.786	2.543	0.243	9.556	6.927
10190	3.292	2.986	0.306	10.248	7.508
10250	3.359	3.083	0.276	8.952	6.420
10310	5.476	5.133	0.343	6.682	4.513
10370	4.693	4.36	0.333	7.638	5.316
10430	3.806	3.545	0.261	7.362	5.084
10490	1.962	1.775	0.187	10.535	7.750
10550	2.421	2.195	0.226	10.296	7.549
10610	2.368	2.185	0.183	8.375	5.935
10670	3.839	3.611	0.228	6.314	4.204
10730	3.654	3.391	0.263	7.756	5.415
10790	2.173	2.013	0.16	7.948	5.577
10850	6.057	4.908	1.149	23.411	18.565
10910	4.058	3.262	0.796	24.402	19.398
10970	3.762	3.077	0.685	22.262	17.600
11030	5.717	4.691	1.026	21.872	17.272
11090	5.291	4.425	0.866	19.571	15.339
11150	6.55	5.133	1.417	27.606	22.089

Appendix D - Weight percent of calculated mineralogy

The graphs of the XRD bulk powder results of the 2Θ and d-spacing of peaks were analyzed and measured to determine which mineral peaks were present. The data from the HHXRF provides the elemental weight percent, which is the percentage of the weights of the various elements within the sample compared to the total sample weight. The elemental weight percent is divided by the molar weight of each element, thus calculating the molar proportion (element weight percent/atomic mass = molar proportion). To calculate the atomic weight percentage, the molar proportion for all the elements analyzed is summed and each element's molar weight is then divided by their total weight (element's molar proportion/total of all the samples molar proportion = element atomic weight percent).

The elements that were used in this study were Al, Si, P, S, K, Ca Ti, and Fe. The elements of V, Cr, and Mn are ignored, because they are only present in trace amounts within the identified Woodford Shale. Mg was not used, because the data produced by HHXRF have a high analytical uncertainty (x%). For this reason, the abundances of Mg-bearing minerals, such as chlorite and dolomite cannot be accurately determined.

After the atomic weight percent is calculated, it is possible to calculate the mineral weight percent. The XRD defined the mineralogy of each sample and the HHXRF defined what elements and how much of said elements are in each sample. The calculated mineral weight percentages provide an estimation of the mineral proportions in each sample—with the caveat above about underestimation of Mg-bearing minerals. The first step is to calculate the atomic weight percent of the mineral. This is accomplished by determining the least abundant element within each type of mineral, based on the elemental structure of the mineral within the limitations stated above. Take the atomic weight percent for that element of that sample and

factor it so the chosen element corresponding to the mineral make up reflects one atom of said element minus the atomic weight of any other minerals that uses the same element factored so the atomic weight reflects the full quantity of the element within the mineral. The next step is to find the molar proportion by taking to atomic weight percent times the mineral mole mass to derive the molar proportion. To calculate the mineral weight percent, take the molar proportion of the mineral and divide it by the sum of all the mineral molar proportion for the sample.

The first mineral that is calculated is illite, $(KAl_2(Si,Al)_4O_{10})$, this is derived from the atomic weight percent of K. The second mineral that is calculated is pyrite, (FeS_2) , this is derived from the atomic weight percent of S divided by two because it takes two moles of S to make one pyrite. The third mineral that is calculated is apatite, $(Ca_5(PO_4)_3(OH,F,Cl))$, this is derived from the atomic weight percent of P divided by three because it takes three moles of P to make one mole of apatite. The fourth mineral that is calculated is Fe-Ti oxide, $(FeTiO_3)$, this is derived from the atomic weight percent of Ti. The fifth mineral that is calculated is dolomite, $(Ca,Mg)CO_3$, this is derived from the atomic weight percent of calcium subtracted from the calculated atomic weight percent of apatite. The sixth mineral that is calculated is chlorite, $((Mg, Fe)_4Al_4Si_2O_{10}(OH)_8)$, this is derived from the atomic weight percent of Fe subtracted from the calculated atomic weight percent of pyrite divided by four and the atomic weight percent of Fe-Ti Oxide divided by four. The final and seventh mineral that is calculated is quartz, (SiO_2) , this is derived from the atomic weight percent of silicon subtracted from calculated atomic weight percent illite times two and from calculated atomic weight percent of chlorite times three. This process is repeated for each of the 75 samples.

Sample	Wt % of calculated mineralogy							TOC	Mineral BI
	illite	pyrite	FeTi oxides	apatite	chlorite	dolomite	quartz		
6820	24.33	1.03	1.69	0.12	14.95	5.04	52.85	5.82	0.56
6880	28.13	1.06	1.87	0.05	15.10	6.89	46.90	8.60	0.51
6910	29.82	1.15	1.90	0.06	14.00	6.79	46.27	9.17	0.50
6940	28.74	1.29	1.91	0.07	13.28	7.33	47.37	9.49	0.52
7000	27.37	1.25	1.79	0.07	12.73	5.77	51.02	15.08	0.51
7060	26.33	1.32	1.70	0.13	11.41	8.12	50.98	8.15	0.56
7120	29.34	1.20	1.86	0.11	13.08	5.83	48.59	11.15	0.50
7180	17.73	0.92	1.35	0.13	9.87	7.46	62.54	11.35	0.64
7250	20.35	1.45	1.37	0.18	9.02	9.27	58.37	11.25	0.62
7310	28.28	1.40	1.79	0.11	11.91	8.04	48.46	10.77	0.53
7370	30.09	1.42	1.86	0.09	12.62	7.02	46.89	7.73	0.52
7430	25.19	1.84	1.55	0.18	9.14	9.65	52.45	18.02	0.54
7490	26.93	1.17	1.73	0.09	10.56	5.91	53.62	46.72	0.41
7550	0.00	0.00	0.00	0.00	0.00	0.00	0.00	0.00	0.00
7610	0.00	0.00	0.00	0.00	0.00	0.00	0.00	0.00	0.00
7670	0.00	0.00	0.00	0.00	0.00	0.00	0.00	0.00	0.00
7730	0.00	0.00	0.00	0.00	0.00	0.00	0.00	0.00	0.00
7790	0.00	0.00	0.00	0.00	0.00	0.00	0.00	0.00	0.00
7850	0.00	0.00	0.00	0.00	0.00	0.00	0.00	0.00	0.00
7910	0.00	0.00	0.00	0.00	0.00	0.00	0.00	0.00	0.00
7970	21.69	5.10	0.98	0.62	27.28	2.15	42.19	8.24	0.44
8030	28.98	5.20	1.07	0.46	1.71	0.69	61.89	8.45	0.62
8090	29.01	5.16	1.06	0.47	1.68	0.60	62.02	8.66	0.61
8150	29.47	5.22	1.09	0.48	1.82	0.81	61.11	9.30	0.60
8180	29.12	5.15	1.08	0.48	1.74	0.95	61.48	9.58	0.61
8210	28.58	5.15	1.05	0.51	1.59	1.42	61.71	8.58	0.62
8270	28.33	5.08	1.05	0.44	1.70	2.70	60.69	6.18	0.64
8330	29.64	1.11	1.84	0.12	13.32	8.07	45.89	6.62	0.52
8390	29.79	1.14	1.87	0.11	12.75	8.79	45.55	7.22	0.52
8450	29.25	1.40	1.88	0.11	12.96	8.28	46.12	8.18	0.52
8510	31.45	1.25	1.97	0.12	14.33	7.34	43.54	6.37	0.49
8570	32.37	1.14	2.00	0.11	14.59	7.47	42.31	6.85	0.48
8630	32.66	1.14	2.04	0.08	14.81	7.01	42.25	7.05	0.47
8690	32.32	1.26	2.07	0.08	15.14	8.69	40.45	9.39	0.46
8750	31.86	1.64	1.98	0.11	14.25	9.25	40.91	9.06	0.48
8810	31.54	1.53	1.98	0.08	14.27	9.32	41.28	6.35	0.49
8870	21.95	1.08	1.58	0.09	14.47	7.25	53.59	6.11	0.59
8930	21.95	1.01	1.54	0.14	16.94	7.49	50.93	5.99	0.57
8990	21.53	1.14	1.53	0.13	12.95	7.38	55.32	7.06	0.60

Sample	Wt % of calculated mineralogy							TOC	Mineral BI
	illite	pyrite	FeTi oxides	apatite	chlorite	dolomite	quartz		
9050	21.61	1.04	1.45	0.16	14.09	6.98	54.68	6.68	0.59
9110	23.62	1.07	1.58	0.18	15.85	5.20	52.49	6.23	0.56
9170	22.46	0.96	1.53	0.15	15.46	4.73	54.71	6.84	0.57
9230	24.43	1.08	1.72	0.09	16.00	5.27	51.42	6.98	0.54
9290	29.87	1.07	1.93	0.05	14.25	7.77	45.06	7.13	0.51
9350	30.16	1.15	1.92	0.07	14.12	6.35	46.22	7.63	0.50
9410	27.60	1.41	1.89	0.06	12.60	7.88	48.55	6.75	0.55
9470	27.80	1.17	1.78	0.08	12.95	4.81	51.40	7.21	0.54
9530	25.31	1.44	1.61	0.15	10.44	8.90	52.15	6.23	0.59
9590	31.83	1.01	2.02	0.08	14.79	5.12	45.15	6.78	0.48
9650	11.62	0.87	1.07	0.16	7.76	8.35	70.16	4.80	0.76
9710	24.94	1.77	1.52	0.18	9.55	9.72	52.32	5.77	0.61
9770	33.01	1.02	2.08	0.04	15.01	4.93	43.91	7.47	0.47
9830	24.03	2.10	1.46	0.21	8.33	11.47	52.40	6.05	0.62
9890	28.05	1.19	1.78	0.07	10.88	5.68	52.35	6.39	0.56
9950	25.32	1.17	1.63	0.13	10.22	6.23	55.30	7.23	0.59
10010	20.72	2.17	2.38	0.24	12.22	12.62	49.66	5.63	0.62
10070	22.07	2.56	2.19	0.26	10.22	11.89	50.82	3.96	0.63
10130	22.61	2.80	2.24	0.19	9.90	10.50	51.77	6.93	0.61
10190	22.18	2.72	2.23	0.17	10.60	11.78	50.32	7.51	0.61
10250	27.34	1.70	1.93	0.12	13.21	9.98	45.72	6.42	0.54
10310	30.33	1.11	1.89	0.11	13.55	7.96	45.06	4.51	0.52
10370	29.35	1.14	1.84	0.12	12.99	8.73	45.83	5.32	0.53
10430	29.87	1.31	1.92	0.10	12.90	8.44	45.47	5.08	0.53
10490	30.34	1.34	1.91	0.14	13.81	7.49	44.98	7.75	0.50
10550	32.31	1.13	1.98	0.11	14.50	7.47	42.51	7.55	0.48
10610	32.31	1.17	2.03	0.09	14.60	7.18	42.62	5.94	0.49
10670	32.91	1.18	2.08	0.08	15.17	7.99	40.60	4.20	0.48
10730	31.88	1.56	2.00	0.09	14.51	9.23	40.74	5.41	0.49
10790	31.69	1.55	2.00	0.09	14.30	9.19	41.18	5.58	0.49
10850	25.00	1.25	1.68	0.09	14.08	8.05	49.84	18.57	0.50
10910	22.02	1.02	1.55	0.12	16.64	7.30	51.34	19.40	0.50
10970	21.53	1.16	1.53	0.14	13.96	7.66	54.03	17.60	0.54
11030	21.69	1.00	1.47	0.13	14.01	6.99	54.71	17.27	0.54
11090	23.03	1.08	1.56	0.19	14.54	5.81	53.80	15.34	0.53
11150	22.15	0.99	1.53	0.17	16.69	4.97	53.51	22.09	0.49